POLITECNICO DI TORINO
Repository ISTITUZIONALE

Deadbeat Direct Flux Control: Plug-and-Play Torque Controllers for Electrically Excited Synchronous Motors

Original
Deadbeat Direct Flux Control: Plug-and-Play Torque Controllers for Electrically Excited Synchronous Motors / Rubino, S., Ionta, A., Graffeo, F., Bojoi, R.. - In: IEEE TRANSACTIONS ON POWER ELECTRONICS. - ISSN 0885-8993. - (2026), pp. 1-19. [10.1109/TPEL.2026.3696740]

Availability:
This version is available at: 11583/3011410 since: 2026-05-26T17:41:28Z

Publisher:
IEEE

Published
DOI:10.1109/TPEL.2026.3696740

Terms of use:

This article is made available under terms and conditions as specified in the corresponding bibliographic description in the repository

Publisher copyright
IEEE postprint/Author's Accepted Manuscript

©2026 IEEE. Personal use of this material is permitted. Permission from IEEE must be obtained for all other uses, in any current or future media, including reprinting/republishing this material for advertising or promotional purposes, creating new collecting works, for resale or lists, or reuse of any copyrighted component of this work in other works.

(Article begins on next page)

03 November 2026

This article has been accepted for publication in IEEE Transactions on Power Electronics. This is the author's version which has not been fully edited and content may change prior to final publication. Citation information: DOI 10.1109/TPEL.2026.3696740

Deadbeat Direct Flux Control: Plug-and-Play Torque Controllers for Electrically Excited Synchronous Motors

Sandro Rubino, *Senior Member, IEEE*, Alessandro Ionta, *Student Member, IEEE*, Federica Graffeo, *Member, IEEE* and Radu Bojoi, *Fellow, IEEE*

***Abstract*—Permanent magnet synchronous machines (PMSMs) have long been regarded as the benchmark technology for electric powertrains due to their superior torque density and efficiency. However, the growing demand to reduce reliance on rare-earth materials has drawn attention to electrically excited synchronous machines (EESMs) as a competitive alternative for traction applications. EESMs offer greater control flexibility, as their magnetic flux can be actively regulated and optimized via the rotor field current. However, limited control solutions are reported in the literature, primarily based on current vector controllers and only partially addressing optimal torque regulation. Furthermore, the cross-coupling introduced by the magnetic interaction between stator and rotor increases the complexity of the inner loops' design, whose performance is significantly affected by the magnetic saturation. As a consequence, EESM drives for traction applications often require the execution of demanding calibration and certification procedures. Therefore, this article proposes cutting-edge self-calibrated torque controllers for traction EESMs based on a deadbeat direct flux control (DB-DFC) approach. The proposed solution eliminates the need for any tuning efforts for the inner control loops while achieving high-performance of torque regulation and minimizing the overall copper losses, thus resulting in plug-and-play torque controllers. The experimental validation is carried out on a 100 kW commercial EESM used in the Renault Zoe EV R135, confirming the effectiveness and the added value of the proposed torque controllers in traction applications.**

***Index Terms*—electrically excited synchronous machine, traction, electric vehicles, torque control, deadbeat.**

I. Introduction

THE rapid expansion of hybrid and fully electric traction powertrains has intensified the demand for electrical machines that combine high performance with competitive cost. Currently, permanent magnet synchronous machines (PMSMs) represent the predominant technology, primarily because of their superior power and torque density [1]. However, their reliance on rare-earth permanent magnets raises critical concerns related to cost volatility, supply chain security, and environmental sustainability. These limitations have motivated extensive research into magnet-free alternatives capable of achieving comparable performance without such material dependency.

Among these alternatives, the electrically excited synchronous machine (EESM) has emerged as a promising solution for traction applications. Unlike PMSMs, the EESM's excitation field is generated by supplying direct current to a rotor winding, thereby completely eliminating permanent magnets. This configuration inherently avoids key PMSM-related risks such as demagnetization and uncontrolled generation, while simultaneously providing operational flexibility. Specifically, the capability to regulate the magnetic flux through the rotor field current enables optimal flux weakening and extended constant-power operation across a wide speed range [2]. These features have driven growing interest among automotive manufacturers, who are increasingly exploring and adopting EESM topologies for next-generation powertrains [3]–[5].

Despite these advantages, EESMs introduce specific challenges in torque control [6]. A central difficulty arises from the magnetic coupling between the stator d-axis current and the rotor excitation field, resulting in cross-coupling effects that complicate independent current regulation and make it necessary to implement advanced control algorithms [7]. Moreover, traction EESM design procedures typically result in an inductance of the rotor excitation winding that is much higher than the stator inductances. As a result, the excitation circuit exhibits considerably slower dynamics even under maximum excitation voltage compared to the rapid response of stator currents. Achieving optimal trajectories further requires frequent adjustments of the excitation current, thereby limiting torque response capabilities [8]. Thermal management techniques can partially mitigate these constraints by allowing temporary increases in stator current during transients, thus leveraging the faster stator dynamics to enhance torque responsiveness [9]. However, such methods remain restricted to short-term operation. Consequently, a robust and general solution must explicitly consider, and effectively exploit, the intrinsic coupling between stator and rotor magnetic fields [10].

In the literature, several control strategies have been investigated [11]–[15] to solve the aforementioned issues. A current vector control (CVC) scheme is presented in [16], where the benefits of modeling the machine in a stator flux-oriented reference frame are emphasized. Alternative approaches that directly regulate the stator flux [17], [18] demonstrate that avoiding direct control of the stator d-axis current mitigates stator–rotor coupling effects and improves torque regulation. Nevertheless, the solutions in [17], [18] require parameter-dependent regulator tuning, and their dynamic performance is inherently linked to regulator bandwidth and, consequently, the sampling frequency of the digital control unit.

Considering PMSMs drives, deadbeat (DB) control strategies have demonstrated the ability to achieve the commanded torque response within two sampling periods [19], [20],

Authorized licensed use limited to: Politecnico di Torino. Downloaded on May 26,2026 at 17:03:39 UTC from IEEE Xplore. Restrictions apply.
© 2026 IEEE. All rights reserved, including rights for text and data mining and training of artificial intelligence and similar technologies. Personal use is permitted, but republication/redistribution requires IEEE permission. See https://www.ieee.org/publications/rights/index.html for more information.

This article has been accepted for publication in IEEE Transactions on Power Electronics. This is the author's version which has not been fully edited and content may change prior to final publication. Citation information: DOI 10.1109/TPEL.2026.3696740

provided that voltage and current constraints of the power converter are not involved. Moreover, DB solutions can operate with low sampling-to-fundamental frequency ratios when the control variables, such as torque and currents, are correctly predicted. Further, their well-defined behavior under voltage and current limits represents a clear advantage over conventional solutions adopting synchronous reference frame regulators like proportional-integral ones. Building on this, deadbeat- direct torque and flux control (DB-DTFC) strategies have been proposed in [21], [22] for EESMs, where the field flux linkage reference is derived to achieve unity power factor in steady-state operation. However, operation at unity power factor does not necessarily minimize machine losses, and achieving higher efficiency requires more sophisticated control algorithms [8], [9], [23]–[27]. Furthermore, DB-DTFC schemes typically rely on current estimators [20], thereby increasing system complexity. According to the presented state-of-the-art, the literature on EESM drives for traction does not report torque control solutions that do not require calibration of the inner control loops, regardless of whether these last adopt PI or DB regulators, due to their performance being dependent on the machine's inductances, i.e., the magnetic saturation.

In this context, this article proposes torque controllers based on the direct control of the machine's stator and rotor fluxes using DB regulators. This way, the dynamic performance of torque regulation is immune to the magnetic saturation and sampling frequency of the digital controller. Indeed, the state-space equations for the stator and rotor flux linkages are straightforward to discretize accurately. A direct consequence of these advantages is the possibility of avoiding calibration and certification procedures for the inner flux control loops, regardless of whether steady-state or fast-transient torque regulation scenarios are performed. The proposed solutions achieve torque accuracy by combining specific control maps that provide rotor and stator flux references based on the torque request, with error-compensating integral mechanisms whose reaction time is arbitrarily defined. This way, potential errors in computing the control maps due to mismatches in the machine's inductances are automatically compensated, resulting in non-critical errors in torque regulation accuracy. Moreover, the proposed solutions are based on a control structure that allows optimal torque control by minimizing the overall copper losses, thus satisfying the high efficiency requirements of traction drives.

According to the literature, the stator flux linkage of ac motors can be controlled considering different approaches. On the one hand, advanced solutions based on flux vector control in rotor dq and stationary $\alpha\beta$ coordinates are reported for PMSM drives [28], [29]. However, recent torque controllers based on the polar control of the stator flux vector, i.e., amplitude and load angle, have been proposed by exploiting the stator dqs coordinates [30]. However, the application of these direct flux control approaches on EESM is not reported in the literature, including a comparison of the torque regulation performance obtained with them. In summary, this article proposes plug-and-play torque controllers for EESM based on a ead-beat direct flux control (DB-DFC) approach.

This article thus advances the state of the art in EESM torque control through the following contributions.

- The first self-calibrated torque controllers for traction EESM drives are proposed, allowing the elimination of the need for demanding tuning and deployment procedures.
- The first torque controllers for traction EESM drives based on the direct control of both the stator and rotor machine's fluxes are proposed, enabling ultra-high dynamic performance of torque regulation while minimizing overall Joule losses.
- The first attempt in the literature to implement and compare, for traction EESM drives, the most adopted direct flux control approaches using DB regulators. In detail, flux vector control strategies in stationary $\alpha\beta$ and rotor dq coordinates, as well as the more recent flux polar control strategy in stator dqs coordinates, are considered.
- A detailed experimental analysis of the torque regulation performance obtained by the proposed DB-DFC strategies is reported, considering the effect of low sampling-to-fundamental frequency ratios and typical mismatch of the control maps, proving the robustness and the added value of the proposed solutions.

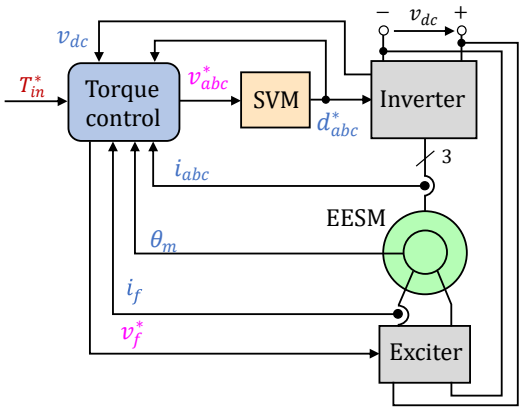


Fig. 1: Schematic view of the considered EESM drive topology.

As illustrated in Fig. 1, the EESM is supplied on the stator side by a voltage-source inverter and on the rotor side by an exciter. The proposed torque controllers provide the reference stator voltages v^*_{abc} for inverter duty-cycle generation, together with the reference field voltage v^*_f for the exciter. The effectiveness of the approach is demonstrated experimentally on a commercial 100 kW EESM integrated in the Renault Zoe EV R135.

The article is organized as follows. Section II provides a comprehensive formulation of the machine model in multiple reference frames and describes the theoretical background. Section III presents an in-depth description of the proposed torque controllers' architecture. Extensive experimental validation is reported in Section IV. Finally, Section V summarizes the main findings and outlines future research developments.

II. EESM MODELING

EESMs can be described in different reference frames, namely the stationary $\alpha\beta$, the rotor dq, and the stator dqs

Authorized licensed use limited to: Politecnico di Torino. Downloaded on May 26,2026 at 17:03:39 UTC from IEEE Xplore. Restrictions apply.
© 2026 IEEE. All rights reserved, including rights for text and data mining and training of artificial intelligence and similar technologies. Personal use is permitted, but republication/redistribution requires IEEE permission. See https://www.ieee.org/publications/rights/index.html for more information.

This article has been accepted for publication in IEEE Transactions on Power Electronics. This is the author's version which has not been fully edited and content may change prior to final publication. Citation information: DOI 10.1109/TPEL.2026.3696740

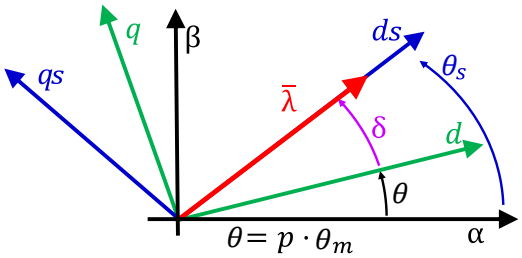


Fig. 2: Schematic view of the stationary- $\alpha\beta$, rotor- dq, and stator- dqs frames for a generic synchronous motor.

coordinates. In the stator flux-oriented frame, the ds-axis is aligned with the stator flux linkage vector $\bar{\lambda}$, as illustrated in Fig. 2. The angular displacement between the stator flux and the rotor d-axis is defined as the machine's load angle δ.

A. Stator voltage model in stationary $\alpha\beta$ coordinates

The stator voltage equation in the stationary $\alpha\beta$ frame is written as [31]:

$$\bar{v}_{\alpha\beta} = R \cdot \begin{bmatrix} i_\alpha \\ i_\beta \end{bmatrix} + \frac{d}{dt} \begin{bmatrix} \lambda_\alpha \\ \lambda_\beta \end{bmatrix} \tag{1}$$

where v, i, and λ denote the stator voltage, current, and flux linkage components, respectively. Considering a discrete-time domain, the following discrete form of (1) is straightforwardly obtained:

$$\bar{v}^k_{\alpha\beta} = R \cdot \begin{bmatrix} i^k_\alpha \\ i^k_\beta \end{bmatrix} + \frac{1}{T_s} \begin{bmatrix} \lambda^{k+1}_\alpha - \lambda^k_\alpha \\ \lambda^{k+1}_\beta - \lambda^k_\beta \end{bmatrix} \tag{2}$$

where T_s is the sampling period while k stands for the generic sampling time instant. It is noted that the stationary coordinates ensure decoupling between the α- and β-axes voltages.

B. Stator voltage model in rotor dq coordinates

The stator voltage equation in the rotor dq reference frame is expressed as [31]:

$$\bar{v}_{dq} = R \cdot \begin{bmatrix} i_d \\ i_q \end{bmatrix} + \frac{d}{dt} \begin{bmatrix} \lambda_d \\ \lambda_q \end{bmatrix} + \omega \cdot \begin{bmatrix} -\lambda_q \\ \lambda_d \end{bmatrix} \tag{3}$$

where ω is the rotor synchronous speed. In discrete-time form, (3) is expressed as:

$$\bar{v}^k_{dq} = R \cdot \begin{bmatrix} i^k_d \\ i^k_q \end{bmatrix} + \frac{1}{T_s} \begin{bmatrix} \lambda^{k+1}_d - \lambda^k_d \\ \lambda^{k+1}_q - \lambda^k_q \end{bmatrix} + \omega^k \cdot \begin{bmatrix} -\lambda^k_q \\ \lambda^k_d \end{bmatrix} \tag{4}$$

C. Stator voltage model in stator dqs coordinates

The voltage equation in the stator flux-oriented dqs frame are expressed as [18], [30], [32]:

$$\bar{v}_{dqs} = R \cdot \begin{bmatrix} i_{ds} \\ i_{qs} \end{bmatrix} + \frac{d}{dt} \cdot \begin{bmatrix} \lambda \\ 0 \end{bmatrix} + \lambda \cdot \begin{bmatrix} 0 \\ \omega + \frac{d\delta}{dt} \end{bmatrix} \tag{5}$$

whose discrete-time form is computed as:

$$\bar{v}^k_{dqs} = R \cdot \begin{bmatrix} i^k_{ds} \\ i^k_{qs} \end{bmatrix} + \frac{1}{T_s} \cdot \begin{bmatrix} \lambda^{k+1} - \lambda^k \\ \lambda^k \cdot (\delta^{k+1} - \delta^k) \end{bmatrix} + \begin{bmatrix} 0 \\ \lambda^k \cdot \omega^k \end{bmatrix} \tag{6}$$

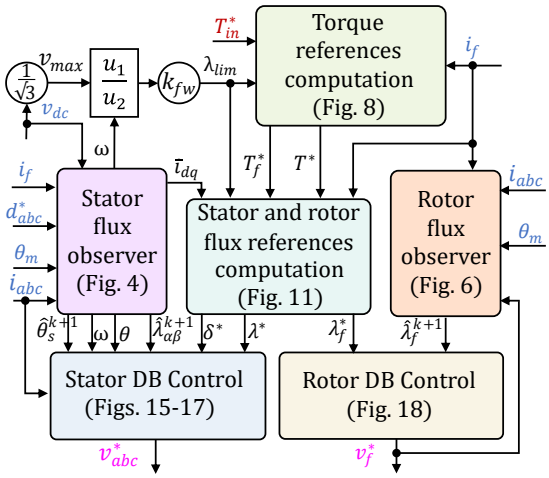


Fig. 3: Schematic view of the proposed torque controller.

D. Rotor voltage model

The EESM allows direct field regulation through the rotor current i_f. The rotor voltage equation is given by:

$$v_f = R_f \cdot i_f + \frac{d}{dt}\lambda_f \tag{7}$$

where the subscript f denotes rotor winding quantities, i.e., voltage v_f, current i_f, flux linkage λ_f, and resistance R_f. The discrete-time form of (7) is written as:

$$v^k_f = R_f \cdot i^k_f + \frac{\lambda^{k+1}_f - \lambda^k_f}{T_s} \tag{8}$$

III. Torque Control Scheme

The overall structure of the proposed DB-DFC torque controllers is shown in Fig. 1 and Fig. 3. Given the input torque reference T^*_{in}, the controller computes the reference stator phase voltages $v^*_{abc} = [v^*_a, v^*_b, v^*_c]$ together with the reference rotor voltage v^*_f. These quantities are obtained by processing multiple feedback signals, including the stator phase currents $i_{abc} = [i_a, i_b, i_c]$, the dc-link voltage v_{dc}, the rotor mechanical position θ_m, and the rotor field current i_f.

The stator reference voltages v^*_{abc} are transformed into inverter duty cycles $d^*_{abc} = [d^*_a, d^*_b, d^*_c]$ through a PWM technique. In this work, a carrier-based space vector modulation (SVM) method is employed [33].

As depicted in Fig. 3, the DB-DFC architecture is organized into six functional modules:

A. Stator flux observer
B. Rotor flux observer
C. Torque references computation
D. Stator and rotor flux references computation
E. Stator DB control
F. Rotor DB control

The operation of these control modules is detailed in the following subsections. For clarity, the following notation is adopted throughout the description of the control architecture: the superscript " ˜ " indicates an estimated quantity, " ˆ " denotes an observed quantity, and " * " specifies a reference value. Estimated quantities arise from open-loop model

Authorized licensed use limited to: Politecnico di Torino. Downloaded on May 26,2026 at 17:03:39 UTC from IEEE Xplore. Restrictions apply.
© 2026 IEEE. All rights reserved, including rights for text and data mining and training of artificial intelligence and similar technologies. Personal use is permitted, but republication/redistribution requires IEEE permission. See https://www.ieee.org/publications/rights/index.html for more information.

This article has been accepted for publication in IEEE Transactions on Power Electronics. This is the author's version which has not been fully edited and content may change prior to final publication. Citation information: DOI 10.1109/TPEL.2026.3696740

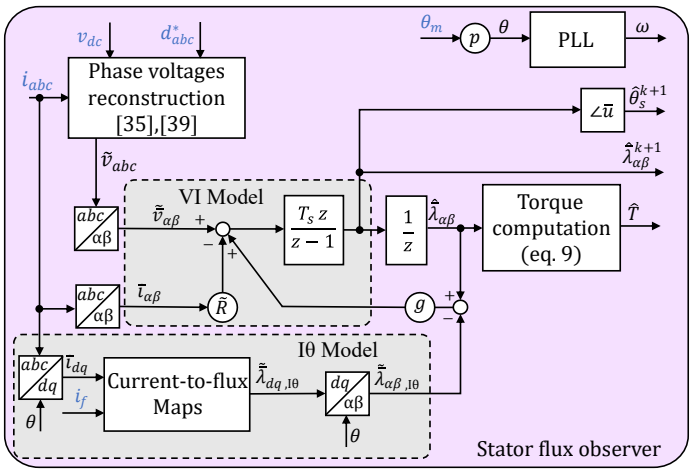


Fig. 4: Schematic view of the adopted stator flux observer.

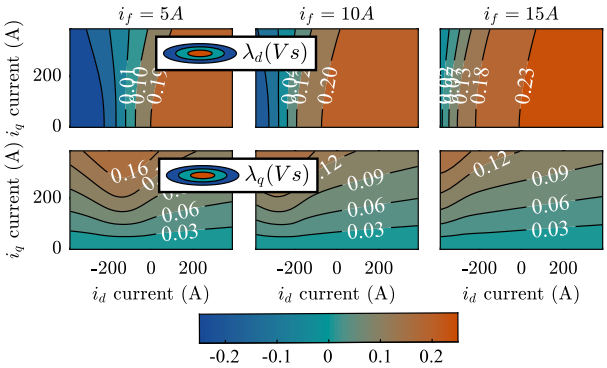


Fig. 5: Stator current-to-flux maps for the EESM under consideration.

propagation, while observed quantities are obtained from closed-loop observers incorporating measurement feedback.

In the following, the superscripts $k+1$ and $k+2$ will be used to denote predicted variables with respect to the considered sampling time instant k. This way, all the variables computed for the latter can be reported without any superscript, simplifying the notation.

A. Stator flux observer

The stator flux vector is evaluated using a hybrid observer that integrates two model-based estimators [32], [34], [35]. Its discrete-time implementation is depicted in Fig. 4.

The observer combines the following estimators.

1) Current model (Iθ): it derives the stator flux from current-to-flux relationships [32], implemented through look-up tables (LUTs) in the control architecture and shown in Fig. 5. These LUTs can also be directly obtained from conventional finite element analysis (FEA), typically executed in traction applications. Alternatively, experimental current-to-flux maps obtained by conventional identification procedures [36], [37] can be adopted, improving torque accuracy at very low speed. The advantages of this estimator mainly include its immunity to stator voltage drops caused by stator resistance and the inverter's voltage errors [32], [34], [35].
2) Voltage model (VI): it estimates the flux via backward Euler integration of the stator back-electromotive force (back-emf). Since this approach inherently predicts the stationary components of the stator flux vector one sampling step ahead [38], a compensating delay is introduced in the feedback loop. The phase voltages $\tilde{v}_{abc}$ are reconstructed from the measured dc-link voltage and the applied duty cycles d^*_{abc} [35], [39]. To account for inverter non-idealities, the error terms $\tilde{v}_{dt,abc}$ are interpolated from LUTs indexed by the measured stator currents i_{abc}, following the procedure in [39]. The advantage of this estimator is that it provides a robust and accurate stator flux estimate in the medium- and high-speed range without requiring knowledge of the current-to-flux relationships, and it allows accurate electromagnetic torque estimation (see Fig. 4).

As shown in Fig. 4, the observer gain g rules the transition between the Iθ model, reliable at low speed, and the VI model, which instead ensures high accuracy at medium and high speed. Additional implementation details are available in [32], [34], [35], [38]–[40] and are not reported here, as they are outside the article's aim.

The stator flux observer provides two key outputs:

- The predicted stator flux vector in the stationary $\alpha\beta$ frame $\hat{\bar{\lambda}}_{\alpha\beta}^{k+1}$ and the corresponding position $\hat{\theta}_s^{k+1}$.
- The actual electromagnetic torque, given by:

$$\hat{T} = \frac{3}{2} \cdot p \cdot \left(\hat{\lambda}_\alpha \cdot i_\beta - \hat{\lambda}_\beta \cdot i_\alpha \right) \tag{9}$$

where p indicates the pole pairs number.

Finally, the electrical speed ω is obtained from the d-axis position using a conventional phase-locked loop (PLL) [41].

B. Rotor flux observer

The proposed torque controllers perform the DB control of the rotor flux linkage. Therefore, the one-step prediction of the rotor flux is necessary. To this end, a dual-model observer, analogous to that employed for the stator flux estimation, is adopted. This approach inherently provides the predicted rotor flux $\hat{\lambda}_f^{k+1}$, as illustrated in Fig. 6.

Similar to the stator flux observer, the current model (Iθ) relies on the rotor current-to-flux relationships, as depicted in Fig. 7. These relationships can be implemented using a LUT typically obtained from FEA due to the complexity of experimentally evaluating this type of map. It is highlighted that the mismatch between this LUT and the EESM's real behaviour is mitigated by implementing a correcting mechanism described in the following sections.

Compared to the stator flux observer, the rotor flux one operates differently since the $I\theta$ estimator provides the flux estimate in steady-state conditions regardless of the speed, and also imposes the state of the backward Euler integrator used by the VI estimator. Conversely, the VI estimator provides the predicted rotor flux only in dynamic scenarios, i.e., during

Authorized licensed use limited to: Politecnico di Torino. Downloaded on May 26,2026 at 17:03:39 UTC from IEEE Xplore. Restrictions apply.
© 2026 IEEE. All rights reserved, including rights for text and data mining and training of artificial intelligence and similar technologies. Personal use is permitted, but republication/redistribution requires IEEE permission. See https://www.ieee.org/publications/rights/index.html for more information.

This article has been accepted for publication in IEEE Transactions on Power Electronics. This is the author's version which has not been fully edited and content may change prior to final publication. Citation information: DOI 10.1109/TPEL.2026.3696740

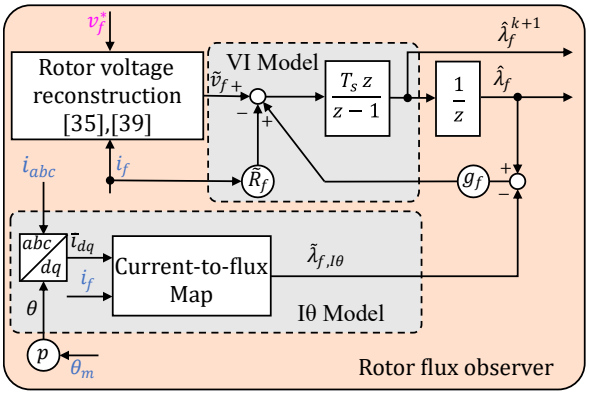


Fig. 6: Schematic view of the adopted rotor flux observer.

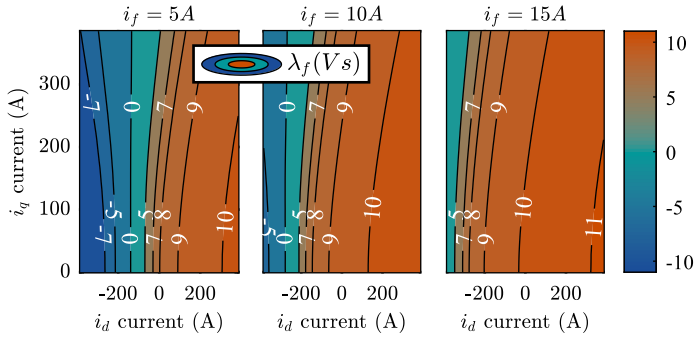


Fig. 7: Rotor current-to-flux maps for the EESM under consideration.

torque transients leading to nonzero time derivatives of the rotor flux. Indeed, the difference between the estimated rotor voltage and the resistive voltage drops is practically zero in steady-state conditions. In other words, the adoption of the VI estimator in the rotor flux observer is justified by the need to obtain a reliable rotor flux prediction in dynamic conditions, allowing for the implementation of a robust DB rotor flux control. Therefore, the observer gain g_f must be set as low as possible to obtain the predicted rotor flux adequately. Also, it is noted that the proposed rotor flux observer provides a flux estimate immune to high-frequency noise introduced by the stator and rotor current measurements. Indeed, the rotor flux estimate corresponds to the output of a pure integrator, which inherently acts as a low-pass filter.

C. Torque references computation

A primary challenge in controlling traction EESMs is the slow response of the rotor excitation system due to its high inductance, whereas stator currents respond much faster. To address this issue, two separate torque references are defined:

1) T_f^*: rotor-side torque reference;
2) T^*: stator-side torque reference.

Torque commands must also comply with the operational limits of the drive system:

$$\begin{cases} i \le i_{max} \\ i_f \le i_{f,max} \\ \lambda \le \lambda_{lim} \le \lambda_{max} \end{cases} \tag{10}$$

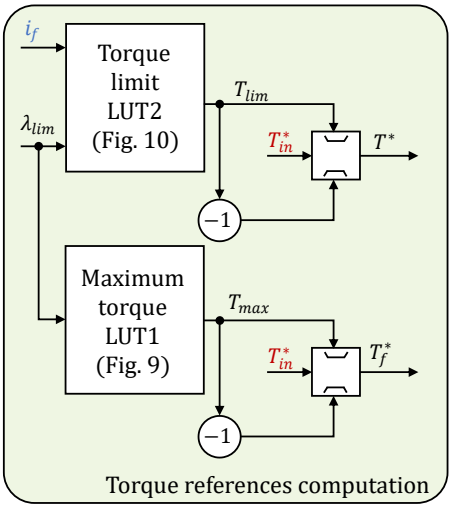


Fig. 8: Schematic view of the torque references computation.

where i_{max} and $i_{f,max}$ are the maximum allowable stator and rotor currents, and λ_{lim} is the flux limit that ensures the inverter voltage constraint is satisfied:

$$\lambda_{lim} = k_{fw} \cdot \frac{v_{max}}{|\omega|}. \tag{11}$$

Here, $v_{max} = v_{dc}/\sqrt{3}$ under SVM, and k_{fw} is a safety factor (typically 0.9–0.95) accounting for inverter non-idealities. Furthermore, λ_{lim} must always remain below the machine's maximum flux λ_{max}, determined by its current-to-flux relationships.

The corresponding control structure, shown in Fig. 8, enables high-performance torque tracking despite slow rotor dynamics.

1) Rotor torque reference T_f^*: The rotor-side torque reference T_f^* is determined by first evaluating the maximum torque T_{max} that the machine can deliver under the instantaneous constraints of λ_{lim}, i_{max}, and $i_{f,max}$. The maximum torque T_{max} is obtained through interpolation of a precomputed one-dimensional LUT1, as shown in Fig. 9. The rotor torque reference is then obtained by limiting the input torque request T_{in}^*:

$$|T_f^*| = \min\left(|T_{in}^*|, |T_{max}|\right). \tag{12}$$

This limitation primarily reflects the stator-side constraints via λ_{lim} and does not explicitly consider the rotor current dynamics.

2) Stator torque reference T^*: The stator-side torque reference T^* must account for the instantaneous rotor current i_f and satisfy the machine's operational constraints (10). To this end, a torque limit T_{lim} is computed, reflecting the machine's actual operational state, as illustrated in Fig. 8. The torque limit T_{lim} is obtained by interpolating the two-dimensional LUT2 with inputs λ_{lim} and i_f, as shown in Fig. 10. This limit allows the stator to temporarily deliver higher stator currents (up to i_{max}) to satisfy fast torque demands while the rotor current changes more slowly. This strategy enhances dynamic performance without exceeding machine or converter limits, ensuring that the efficiency strategy is achieved at steady-state.

Authorized licensed use limited to: Politecnico di Torino. Downloaded on May 26,2026 at 17:03:39 UTC from IEEE Xplore. Restrictions apply.
© 2026 IEEE. All rights reserved, including rights for text and data mining and training of artificial intelligence and similar technologies. Personal use is permitted, but republication/redistribution requires IEEE permission. See https://www.ieee.org/publications/rights/index.html for more information.

This article has been accepted for publication in IEEE Transactions on Power Electronics. This is the author's version which has not been fully edited and content may change prior to final publication. Citation information: DOI 10.1109/TPEL.2026.3696740

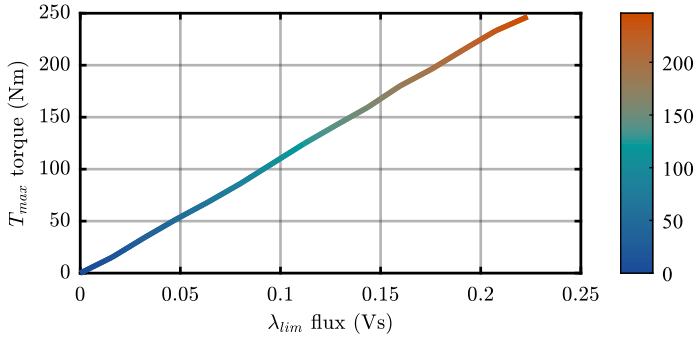


Fig. 9: Maximum torque (T_{max}) profile (LUT1) for the EESM under consideration.

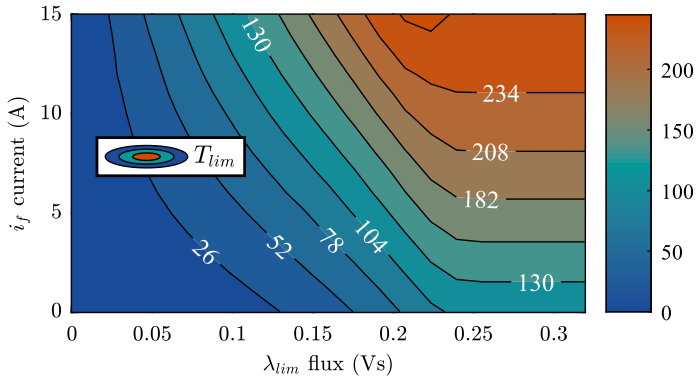


Fig. 10: Torque limit (T_{lim}) map (LUT2) for the EESM under consideration.

D. Stator and rotor flux references computation

Stator and rotor flux references are obtained from the torque references previously computed. Specifically, the stator torque reference T^* is used to determine the stator flux vector references of amplitude λ^* and load angle δ^*. In parallel, the rotor current reference i_f^* is derived from the rotor-side torque reference T_f^* and then converted into the corresponding rotor flux reference λ_f^* through the same current-to-flux map implemented in the rotor flux observer.

It is well established in the literature [8], [9], [23]–[27] that several flux combinations $(\bar{\lambda}^*, \lambda_f^*)$ may satisfy a given torque request T_{in}^*. For simplicity, the proposed torque controllers adopt an efficiency-oriented strategy based on minimizing the overall Joule losses of the machine, comprising both stator and rotor contributions [23]. The optimization is computed using rated values of the stator and rotor resistances. However, the framework can be extended to include temperature dependence by introducing stator and rotor temperature as additional inputs. Furthermore, the same structure could accommodate alternative optimization objectives (e.g., minimizing total Joule plus iron losses or minimizing overall drive losses by including losses contribution of power electronics converters) without requiring changes in the overall controller design. The optimization problem is formulated as:

$$\min_{\lambda,\lambda_f}\left\{\frac{3}{2}\cdot R\cdot i^2 + R_f\cdot i_f^2\right\}, \tag{13}$$

subject to the operational constraints in (10).

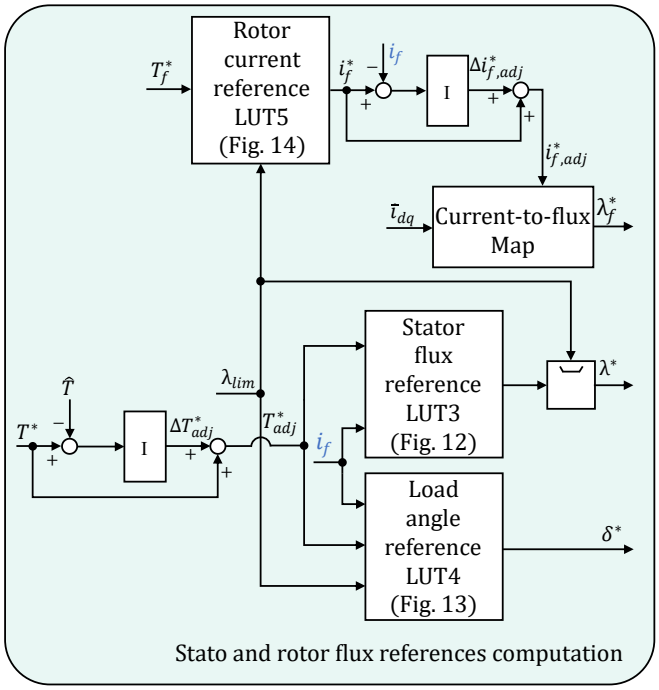


Fig. 11: Schematic view of the stator and rotor flux references computation.

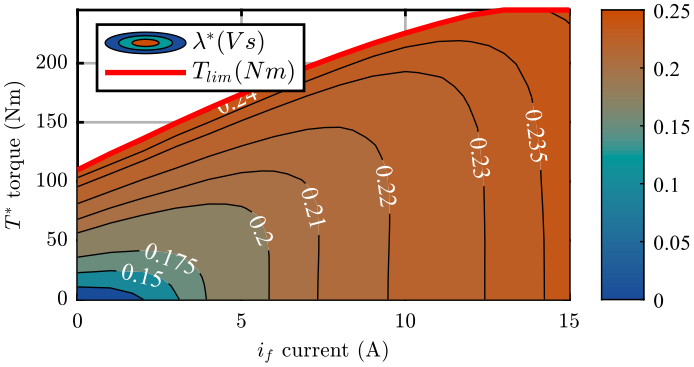


Fig. 12: Flux amplitude reference (λ^*) map (LUT3) for the EESM under consideration.

Solving the minimization problem in real time is impractical due to the nonlinear dependence of the EESM's magnetic behavior on the rotor current i_f. Therefore, (13) is solved offline using the machine's current-to-flux relationships, yielding three precomputed LUTs (LUT3, LUT4, LUT5) that provide the optimal flux amplitude λ^*, load angle δ^*, and rotor current i_f^*, respectively. Representative maps of these LUTs are shown in Figs. 12–14.

It should be noted that the LUT inputs are mutually correlated: the rotor torque reference T_f^* depends on the flux amplitude limit λ_{lim}, while the stator torque reference T^* depends on the instantaneous rotor current i_f. This correlation leads to an irregular map domain, which complicates direct implementation on digital controllers. To overcome this challenge, the normalization approach proposed in [30], [42] and already validated for EESMs in [17], [18] is employed and briefly summarized in the Appendix.

Authorized licensed use limited to: Politecnico di Torino. Downloaded on May 26,2026 at 17:03:39 UTC from IEEE Xplore. Restrictions apply.
© 2026 IEEE. All rights reserved, including rights for text and data mining and training of artificial intelligence and similar technologies. Personal use is permitted, but republication/redistribution requires IEEE permission. See https://www.ieee.org/publications/rights/index.html for more information.

This article has been accepted for publication in IEEE Transactions on Power Electronics. This is the author's version which has not been fully edited and content may change prior to final publication. Citation information: DOI 10.1109/TPEL.2026.3696740

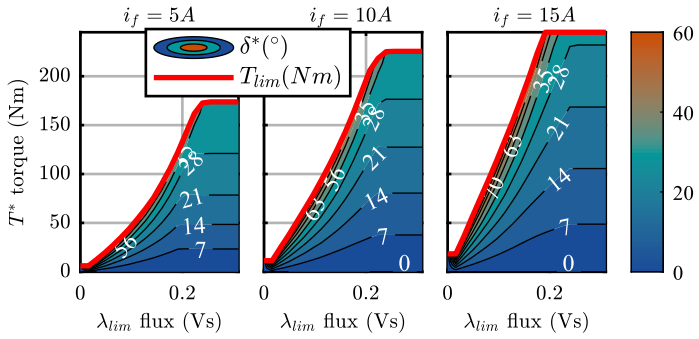


Fig. 13: Load angle reference (δ^*) map (LUT4) for the EESM under consideration.

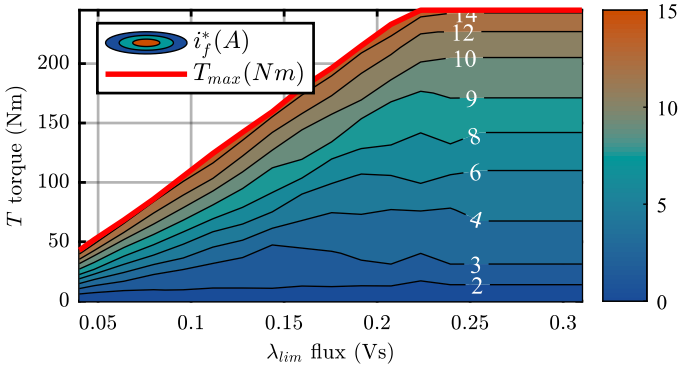


Fig. 14: Rotor current reference (i_f^*) map (LUT5) for the EESM under consideration.

A practical issue arises from inaccuracies in the machine's current-to-flux maps, which may propagate into LUT3-LUT5 and cause steady-state torque errors. Similar limitations are known for current-model-based stator flux observers [32], [34], [35]. Nevertheless, in the medium- and high-speed range, the observer predominantly relies on the voltage model, which is not sensitive to flux map errors. As a result, the observed torque $\hat{T}$ provided by (9) remains accurate in these operating conditions and can be used to evaluate and subsequently compensate potential torque errors.

Therefore, to guarantee high accuracy of steady-state torque regulation, an outer integral correction loop is introduced [28]. This regulator, already proposed for PMSM drives, adjusts the torque reference T^* according to the deviation between the observed torque $\hat{T}$ and the reference one, producing the final reference torque T^*_{adj} provided as input to LUT3 and LUT4 (see Fig. 11). The integrator is designed to operate only in steady state, ensuring convergence of reference torque T^* to the observed one $\hat{T}$, assuming the latter accurate at medium and high speed thanks the implementation of the VI estimator.

The same approach can be employed to ensure the accuracy of the correspondence between the rotor current i_f^* and flux λ_f^* references, using the measured rotor current i_f as feedback of the integral correction loop (see Fig. 11).

The gain of the integral regulator of the aforementioned correction loops corresponds to the reciprocal of the desired reaction time to apply the torque or the rotor current correction, e.g., from 100 to 500 ms. The detailed design of the integral correction loops of torque and rotor current implemented in the proposed torque controllers is reported in the experimental section.

E. DB control

It is well known that a digital controller introduces a one-step execution delay between the computation of the reference voltages and their application via PWM. Therefore, considering the generic sampling time instant k, the machine's variables (currents, fluxes and torque) of the next sampling time instant $k+1$ are already established by the reference voltages computed at the previous sampling time instant $k-1$. Consequently, the reference voltages computed at the generic sampling instant k establish the machine's variables at the sampling time instant $k+2$. The DB approach thus computes the reference voltages by using the discrete-time state-space equations of the controlled variables and by correlating the sampling time instants $k+1$ and $k+2$. Therefore, the proposed torque controllers should compute the reference voltages to be applied at the sampling time instant $k+1$ by setting the rotor and stator fluxes at the sampling time instant $k+2$ equal to their corresponding references. The following discrete-time state-space equations are thus derived from (2), (4), (6), (8).

$$\bar{v}^*_{\alpha\beta} = R \cdot \begin{bmatrix} i_\alpha^{k+1} \\ i_\beta^{k+1} \end{bmatrix} + \frac{1}{T_s} \begin{bmatrix} \lambda_\alpha^* - \lambda_\alpha^{k+1} \\ \lambda_\beta^* - \lambda_\beta^{k+1} \end{bmatrix} \tag{14}$$

$$\bar{v}^*_{dq} = R \cdot \begin{bmatrix} i_d^{k+1} \\ i_q^{k+1} \end{bmatrix} + \frac{1}{T_s} \begin{bmatrix} \lambda_d^* - \lambda_d^{k+1} \\ \lambda_q^* - \lambda_q^{k+1} \end{bmatrix} + \omega^{k+1} \cdot \begin{bmatrix} -\lambda_q^{k+1} \\ \lambda_d^{k+1} \end{bmatrix} \tag{15}$$

$$\bar{v}^*_{dqs} = R \cdot \begin{bmatrix} i_{ds}^{k+1} \\ i_{qs}^{k+1} \end{bmatrix} + \frac{1}{T_s} \cdot \begin{bmatrix} \lambda^* - \lambda^{k+1} \\ \lambda^{k+1} \cdot (\delta^* - \delta^{k+1}) \end{bmatrix} + \begin{bmatrix} 0 \\ \lambda^{k+1} \cdot \omega^{k+1} \end{bmatrix} \tag{16}$$

$$v_f^* = R_f \cdot i_f^{k+1} + \frac{\lambda_f^* - \lambda_f^{k+1}}{T_s} \tag{17}$$

It is noted that the above equations require predicting the machine's currents and the electrical speed ω. However, it should be noted that stator resistive voltage drops are typically negligible in traction motors, resulting in significant differences only at low speed; however, the difference between predicted and measured samples is extremely small ($\alpha\beta$-current) or even null (dq and dqs currents) in steady-state conditions. Conversely, predicting the rotor current is not critical, since its dynamic is governed by the rotor time constant, which is much larger than the digital controller's sampling period, regardless of whether dynamics or steady-state torque regulation is considered. Regarding the electrical rotor speed, its prediction is not significant, as mechanical inertia governs its dynamics. Therefore, the proposed torque controllers compute the reference voltages as follows:

$$\bar{v}^*_{\alpha\beta} = R \cdot \begin{bmatrix} i_\alpha^{k} \\ i_\beta^{k} \end{bmatrix} + \frac{1}{T_s} \begin{bmatrix} \lambda_\alpha^* - \lambda_\alpha^{k+1} \\ \lambda_\beta^* - \lambda_\beta^{k+1} \end{bmatrix} \tag{18}$$

Authorized licensed use limited to: Politecnico di Torino. Downloaded on May 26,2026 at 17:03:39 UTC from IEEE Xplore. Restrictions apply.
© 2026 IEEE. All rights reserved, including rights for text and data mining and training of artificial intelligence and similar technologies. Personal use is permitted, but republication/redistribution requires IEEE permission. See https://www.ieee.org/publications/rights/index.html for more information.

This article has been accepted for publication in IEEE Transactions on Power Electronics. This is the author's version which has not been fully edited and content may change prior to final publication. Citation information: DOI 10.1109/TPEL.2026.3696740

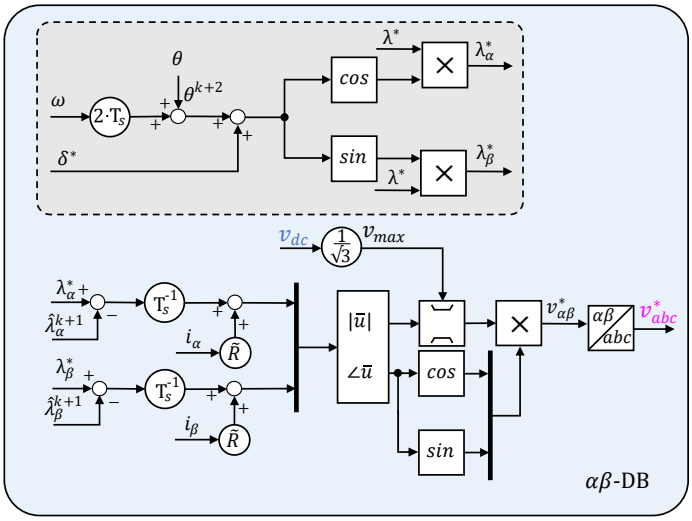


Fig. 15: Schematic view of the $\alpha\beta$-frame based DB approach.

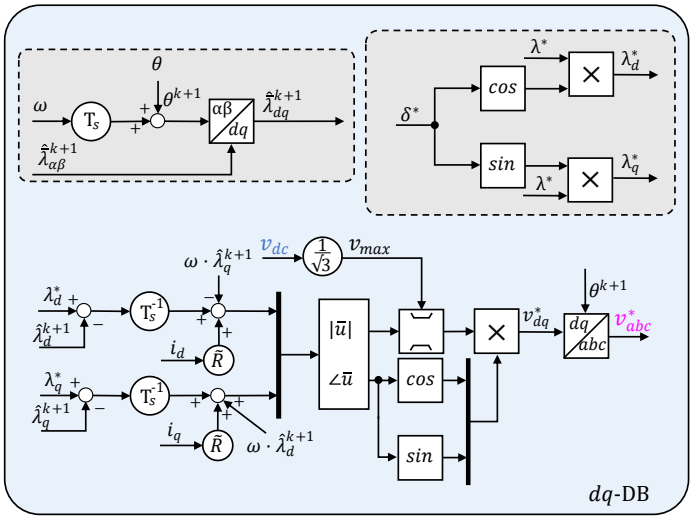


Fig. 16: Schematic view of the dq-frame based DB approach.

$$\bar{v}^*_{dq} = R \cdot \begin{bmatrix} i^k_d \\ i^k_q \end{bmatrix} + \frac{1}{T_s} \begin{bmatrix} \lambda^*_d - \lambda^{k+1}_d \\ \lambda^*_q - \lambda^{k+1}_q \end{bmatrix} + \omega^k \cdot \begin{bmatrix} -\lambda^{k+1}_q \\ \lambda^{k+1}_d \end{bmatrix} \tag{19}$$

$$\bar{v}^*_{dqs} = R \cdot \begin{bmatrix} i^k_{ds} \\ i^k_{qs} \end{bmatrix} + \frac{1}{T_s} \cdot \begin{bmatrix} \lambda^* - \lambda^{k+1} \\ \lambda^{k+1} \cdot (\delta^* - \delta^{k+1}) \end{bmatrix} + \begin{bmatrix} 0 \\ \lambda^{k+1} \cdot \omega^k \end{bmatrix} \tag{20}$$

$$v^*_f = R_f \cdot i^k_f + \frac{\lambda^*_f - \lambda^{k+1}_f}{T_s} \tag{21}$$

It is noted that computing the reference voltages using the above equations has two weaknesses. The first drawback is the execution of fast torque transients at very low speeds, where the above approximation for predicting the stator resistive voltage drop is no longer valid. The second drawback consists of neglecting the voltage errors caused by the dead time introduced by the power electronic converters feeding the motor. These voltage drops are significant at very low speeds, especially for the stator flux control. However, it should be considered that ultra-fast torque transients are rarely performed at very low speeds in real traction applications. In any case, the main effect of the above approximations may be a potential, but not significant, overshoot or undershoot in the stator flux regulation. Conversely, in steady-state conditions, these approximations are automatically compensated for by the outer integral correction loops previously described, which ensure accurate steady-state control of torque and rotor current.

According to the the article's aim, the proposed torque controllers perform the direct control of the stator flux vector in stationary $\alpha\beta$, rotor dq and stator dqs coordinates. In the following, they are thus reported the details on the computation of the reference voltages for each approach.

1) $\alpha\beta$-DB stator flux control: The implementation of the DB control of the stator flux vector in stationary $\alpha\beta$ coordinates is reported in Fig. 15. It is noted that the computation of the $\alpha\beta$ stator flux references requires the double step prediction of the electrical rotor position θ^{k+2}, performed as:

$$\theta^{k+2} = \theta^{k+1} + \omega^{k+1} \cdot T_s \simeq \theta + 2 \cdot \omega \cdot T_s \tag{22}$$

This way, from the references of stator flux amplitude λ^* and load angle δ^*, the corresponding $\alpha\beta$ components of the stator flux vector are computed as:

$$\begin{cases} \lambda^*_\alpha = \lambda^* \cdot \cos(\theta^{k+2} + \delta^*) \\ \lambda^*_\beta = \lambda^* \cdot \sin(\theta^{k+2} + \delta^*) \end{cases} \tag{23}$$

The computation of the $\alpha\beta$ reference voltages is thus performed using (18). However, the amplitude of the reference voltage vector must comply with the inverter's voltage limit v_{max}, making it necessary to limit the computed $\alpha\beta$ reference voltages when performing significant torque transients. Since the $\alpha\beta$ equations are fully decoupled from each other, it is recommended to avoid prioritizing one control axis over the other. Therefore, when performing DB control in $\alpha\beta$ coordinates, voltage limitation is imposed in terms of amplitude while keeping the angle of the reference voltage vector from (18), as shown in Fig. 15. Finally, the references of phase voltages v^*_{abc} are obtained by applying the inverse Clarke transformation on the stationary voltage vector reference $v^*_{\alpha\beta}$.

2) dq-DB stator flux control: The implementation of the DB control of the stator flux vector in rotor dq coordinates is reported in Fig. 16. In this case, the reference components of the stator flux vector are retrieved from the corresponding references of flux amplitude λ^* and load angle δ^* as:

$$\begin{cases} \lambda^*_d = \lambda^* \cdot \cos(\delta^*) \\ \lambda^*_q = \lambda^* \cdot \sin(\delta^*) \end{cases} \tag{24}$$

According to (19), the computation of the dq reference voltages requires the predicted dq components of the stator flux vector. Therefore, the predicted flux estimate $\lambda^{k+1}_{\alpha\beta}$ provided by the observer is expressed in dq coordinates using the rotational transformation according to the predicted rotor electrical position θ^{k+1}. The latter is easily computed as:

$$\theta^{k+1} = \theta + \omega \cdot T_s \tag{25}$$

Authorized licensed use limited to: Politecnico di Torino. Downloaded on May 26,2026 at 17:03:39 UTC from IEEE Xplore. Restrictions apply.
© 2026 IEEE. All rights reserved, including rights for text and data mining and training of artificial intelligence and similar technologies. Personal use is permitted, but republication/redistribution requires IEEE permission. See https://www.ieee.org/publications/rights/index.html for more information.

This article has been accepted for publication in IEEE Transactions on Power Electronics. This is the author's version which has not been fully edited and content may change prior to final publication. Citation information: DOI 10.1109/TPEL.2026.3696740

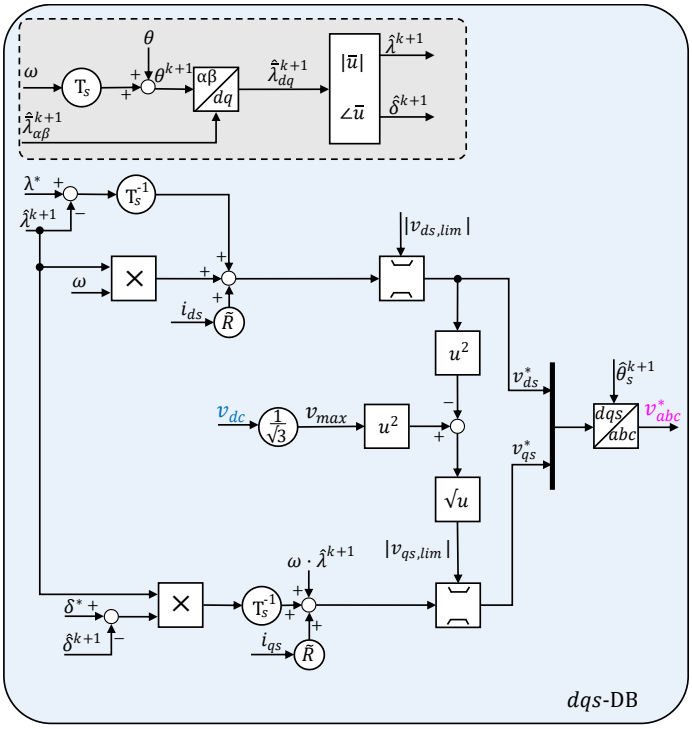


Fig. 17: Schematic view of the dqs-frame based DB approach.

The dq reference voltages are thus computed using (19) and subjected to the constraint of the inverter's voltage limit v_{max}. In this case, the application of this limit is more complex since the dq axes are strongly coupled by the back-emf components ($\omega \cdot \lambda_q$ and $-\omega \cdot \lambda_d$) that, in turn, are modulated by the machine's load angle δ. Ideally, the application of the voltage limit should be performed by prioritizing one control axis over the other according to the machine's operating point. However, establishing the priority is not straightforward when performing rapid and significant torque transients involving a considerable variation in the machine's load angle. Therefore, this article proposes the same voltage limitation approach implemented for the stationary $\alpha\beta$ voltage components. In other words, when performing DB control in dq coordinates, voltage limitation is imposed in terms of amplitude while keeping the angle of the reference voltage vector from (19), as shown in Fig. 16. Subsequently, the references of phase voltages v^*_{abc} are obtained by applying the inverse Park transformation on the dq voltage vector reference v^*_{dq} according to the predicted rotor electrical position θ^{k+1}.

3) dqs-DB stator flux control: The implementation of the DB control of the stator flux vector in stator dqs coordinates is reported in Fig. 17. According to (19), the computation of the dqs reference voltages requires the predicted stator flux amplitude λ^* and load angle δ^*. Therefore, the predicted flux estimate $\hat{\lambda}^{k+1}_{\alpha\beta}$ provided by the observer is first expressed in dq coordinates using the rotational transformation according to the predicted rotor electrical position θ^{k+1} from (25). Subsequently, from the predicted stator flux vector in dq coordinates $\hat{\bar{\lambda}}^{k+1}_{dq}$, the corresponding amplitude $\hat{\lambda}^{k+1}$ and load angle $\hat{\delta}^{k+1}$ are retrieved.

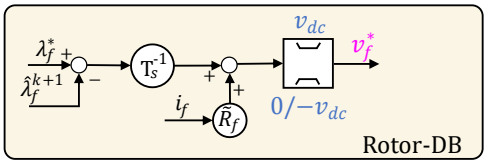


Fig. 18: Schematic view of the DB rotor flux regulator.

TABLE I: Primary data of the EESM under test.

Primary data	
Pole number	4
Peak power	100 kW
Peak torque	245 Nm
Rated power	51 kW
Rated torque	120 Nm
Maximum speed	11000 r/min
Rated dc-link voltage	350 V
Maximum flux (λ_{max})	0.24 Vs
Peak stator current (i_{max})	385 A
Peak rotor current ($i_{f,max}$)	15 A

The dqs reference voltages are thus computed using (20) and subjected to the constraint of the inverter's voltage limit v_{max}. Compared to the previous cases, the two axes are inherently decoupled in this reference frame. Indeed, the stator coordinates dqs have the advantage of focusing all the machine back-emf on a single control axis [30]. Consequently, the machine can be controlled like a separate excited dc motor that presents decoupled mechanisms of flux and torque production. Therefore, only a small margin is required on the ds-axis to compensate for voltage drops caused by stator resistance and voltage errors [30]. Consequently, the qs-axis regulator can exploit nearly the full inverter's voltage range. For practical implementation, the ds-axis limit $v_{ds,lim}$ can be selected following the rule of thumb reported in [30]:

$$2 \cdot R \cdot i_{max} \leq v_{ds,lim} \leq 5 \cdot R \cdot i_{max} \tag{26}$$

Finally, the references of phase voltages v^*_{abc} are obtained by applying the inverse Park transformation on the dqs voltage vector reference v^*_{dqs} according to the predicted stator flux vector position θ^{k+1}_s.

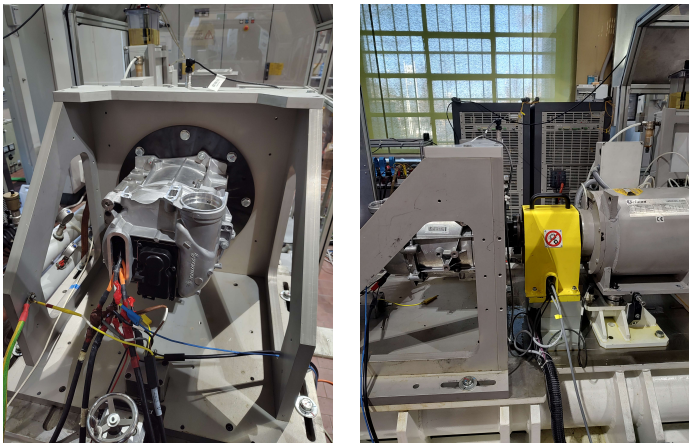
4) Rotor DB flux control: According to Fig. 18, the computation of the reference rotor voltage implementing the DB control of the rotor flux is performed by directly implementing (21). However, the computed reference rotor voltage v^*_f must be limited to comply with the exciter's voltage limit. If considering a bipolar exciter, e.g., a full-bridge converter, the absolute voltage limit corresponds to the dc-link voltage v_{dc}. Conversely, the lower limit of the rotor voltage is zero if a unipolar exciter, e.g., a Buck converter, is used.

IV. Experimental Validation

The experimental validation of the proposed torque controllers has been carried out using as the machine under test (MUT) a commercial sample of the EESM employed in the Renault Zoe EV R135, whose primary data are listed in TABLE I.

Authorized licensed use limited to: Politecnico di Torino. Downloaded on May 26,2026 at 17:03:39 UTC from IEEE Xplore. Restrictions apply.
© 2026 IEEE. All rights reserved, including rights for text and data mining and training of artificial intelligence and similar technologies. Personal use is permitted, but republication/redistribution requires IEEE permission. See https://www.ieee.org/publications/rights/index.html for more information.

This article has been accepted for publication in IEEE Transactions on Power Electronics. This is the author's version which has not been fully edited and content may change prior to final publication. Citation information: DOI 10.1109/TPEL.2026.3696740



(a) (b)

Fig. 19: View of the test rig: (a) EESM under test; (b) EESM coupled with the driving machine.

A. Test rig

The MUT has been tested in torque control mode, with its rotor shaft mechanically coupled to a driving machine (DM) operating as a speed-controlled prime mover, as illustrated in Fig. 19. To ensure high-fidelity torque measurement and rigorously assess the performance of the proposed DB-DFCs, a high-accuracy HBK T12HP torque transducer has been installed between the MUT and the DM.

The stator of the MUT has been supplied by a SiC-based inverter, rated 800 V and 650 A, and operated to the nominal MUT's dc-link voltage of 350 V provided by a bidirectional dc power source. A dedicated IGBT-based full-bridge power module powered the rotor winding. The switching frequencies of the stator inverter and exciter have been set equal to the sampling frequency, implementing a single-edge PWM.

Both the stator inverter and the rotor exciter have been controlled by a dSPACE MicroLabBox platform, responsible for executing the proposed control algorithms, generating PWM signals, and acquiring system measurements for feedback. The control software was fully developed in MATLAB/Simulink, exploiting the dSPACE environment's automatic C-code generation capabilities.

Due to mechanical constraints of the experimental setup, the maximum torque and speed of the MUT have been limited to 150 Nm and 10000 r/min, respectively. Nonetheless, these operating conditions enabled testing the high-power region of the EESM, allowing the MUT to reach its peak power of 100 kW.

B. Experimental results

The proposed DB-DFCs have been experimentally validated on the MUT through a comprehensive test campaign defined to evaluate their performance across the full operational torque-speed range. The experimental tests focused on three key aspects:

- High-torque and deep FW operation: to verify the controllers' capability to fully exploit the MUT's torque and power, including operation in the deep FW region.
- Dynamic torque regulation: to assess the controllers' capability to rapidly follow variable torque commands, including transient responses at constant speed and fast torque reversal with variable speed.
- Steady-state torque control accuracy: to quantify the precision of torque regulation across the entire speed range, ensuring compliance with voltage, current, and flux constraints.

Accordingly, the experimental validation was structured into four representative types of tests:

1) Maximum torque per speed (MTPS) profile;
2) Torque transients;
3) Fast torque reversals;
4) Steady-state torque accuracy.

All tests were conducted using the three DB-DFC approaches considered in this article.

According to the article's contributions, no tuning procedures are needed for the implementation of the proposed torque controller. However, some parameters have to be set as user-specified inputs according to common rules of thumb. The stator g and rotor g_f observer gains have both been set to 20 Hz, corresponding to about 6% of the maximum fundamental frequency of 333 Hz at 10000 r/min. Lower values of observers' gains can be used, provided that an adequate compensation for the power converters' voltage error is implemented in the voltage reconstruction [35], [39]. Indeed, to enhance robustness against current-to-flux map uncertainties, the observer gains should be kept as low as possible, while accounting for the limited back-EMF availability at low speeds, which inherently constrains the reliability of the voltage-model-based estimation. However, any calibration procedure to reduce these gains has been avoided, consistent with the article's aims. Similarly, the voltage margin factor for FW operation has been fixed at k_{fw} = 0.9, although higher values are also possible. The rotor current adjustment integral gain has been tuned to eliminate residual current errors within 0.2 s, yielding a final gain of 5 s^{-1}, while the torque adjustment integral gain has been tuned to eliminate residual torque errors within 0.4 s, leading to an integral gain of 2.5 s^{-1}. Again, these reaction times have been arbitrarily selected without any calibration procedures, although they are more than enough for automotive applications.

The input variables of the control LUTs have been discretized as follows: rotor current i_f from 0 to 15 A ($i_{f,\max}$) with 1 A step, 16 points (pt); flux limit λ_{lim} from 0 to 0.24 Vs ($\lambda_{\max}$) with 0.01 Vs step, 25 pt; Finally, the torque references (T^*, T_f^*) have been discretised between 0 and 245 Nm (peak torque) with a 7 Nm step, 36 points. Therefore, the dimensions of the LUTs were: LUT1 25×1, LUT2 25×16, LUT3 16×36, LUT4 25×36×16, LUT5 25×36. The total memory required for the LUTs is approximately 1 MB. The control algorithms achieved an execution time of about 30 μs on the dSPACE platform. Consequently, the computational efforts of the proposed algorithms ensure their feasibility for deployment on standard automotive-grade microcontrollers. It is highlighted that the implemented LUTs in the proposed torque controllers have been computed from the current-to-

Authorized licensed use limited to: Politecnico di Torino. Downloaded on May 26,2026 at 17:03:39 UTC from IEEE Xplore. Restrictions apply.
© 2026 IEEE. All rights reserved, including rights for text and data mining and training of artificial intelligence and similar technologies. Personal use is permitted, but republication/redistribution requires IEEE permission. See https://www.ieee.org/publications/rights/index.html for more information.

This article has been accepted for publication in IEEE Transactions on Power Electronics. This is the author's version which has not been fully edited and content may change prior to final publication. Citation information: DOI 10.1109/TPEL.2026.3696740

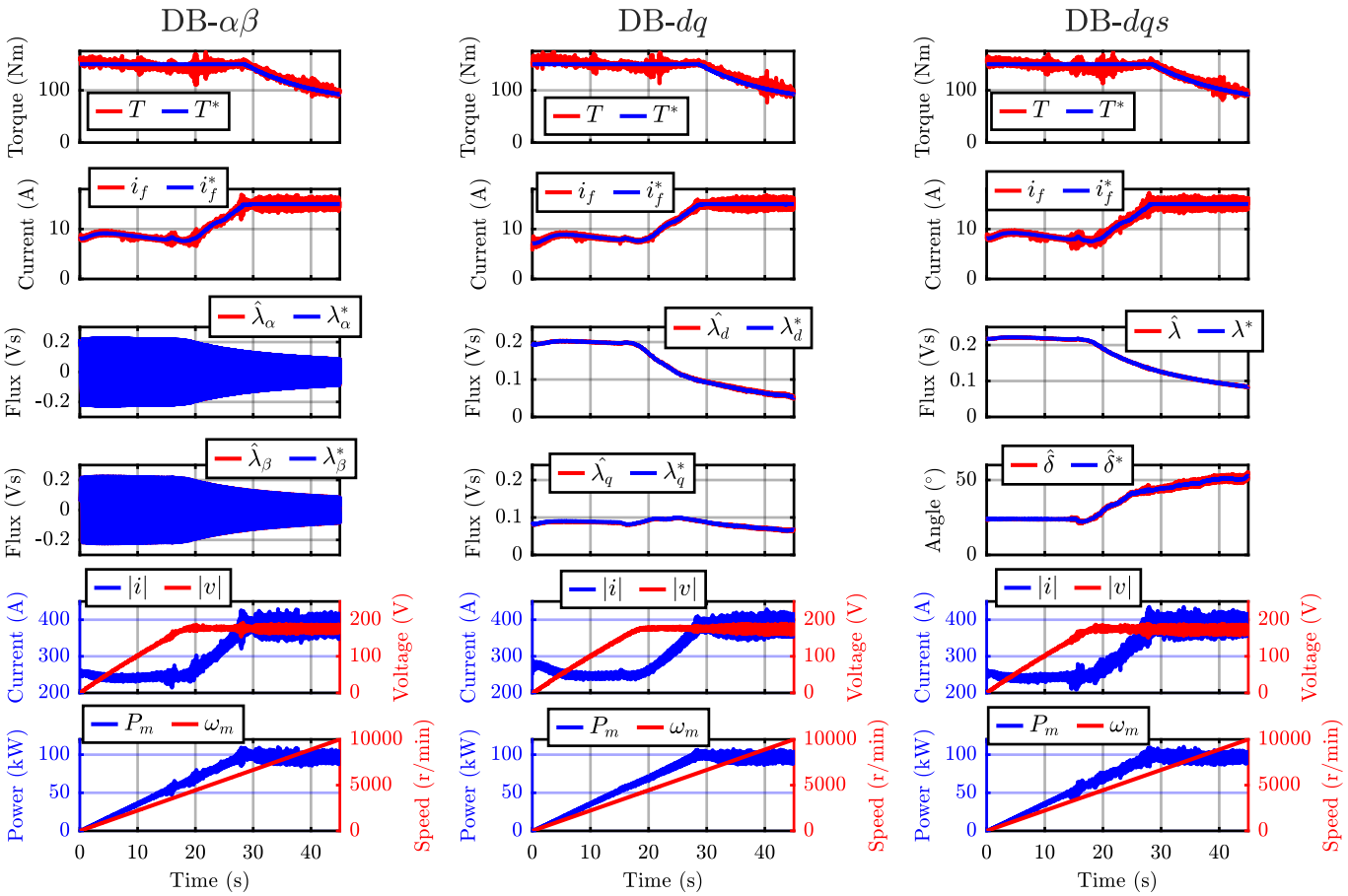


Fig. 20: MTPS profiles: experimental results.

flux maps of the MUT derived solely from FEA [5], [43], [44]. This is typical in the automotive context, where reliable FEA is widely used to avoid time-consuming experimental identification procedures. This choice has enabled efficient testing of the integral correction loops for torque and rotor current under realistic detuning conditions.

The default sampling frequency for all tests has been set at $f_s = 3$ kHz. It is highlighted that at the maximum speed of 10000 r/min, the fundamental frequency of the EESM is 333 Hz, meaning that the sampling-to-fundamental frequency ratio becomes even less than 10, i.e., 9 in this case. This choice has been made to demonstrate the robustness of the proposed torque controllers at a very low sampling-to-fundamental frequency ratio. These experimental tests allow a detailed assessment of both steady-state and dynamic behavior of the controllers, while providing a direct comparison of the different DB implementations under various operational conditions, as discussed in the following subsections.

1) MTPS profile: Starting from standstill, the MUT speed has been progressively increased from zero up to the mechanical limit of the test rig (10000 r/min) using the DM as a speed-controlled prime mover. The acceleration rate has been set to approximately 230 r/min/s to ensure quasi-steady-state conditions throughout the test. During the entire speed ramp, the input torque reference T^*_{in} has been fixed at the maximum permissible value of 150 Nm.

The resulting MTPS profiles obtained with all implemented DB control schemes are presented in Fig. 20. The mechanical power P_m has been computed as the product of the measured torque and speed, both acquired from the torque transducer. The results clearly indicate that, regardless of the adopted DB control approach, the proposed torque controllers fully exploit the MUT's torque and power capabilities across the entire speed range. Moreover, the stator and rotor quantities are accurately regulated in accordance with the total Joule loss minimization criterion, confirming that the DB controllers effectively coordinate multiple physical constraints while ensuring energy-efficient operation.

2) Torque transients: The dynamic behaviour of the proposed torque controllers has been tested by verifying the fast torque transient response at a constant speed of 4000 r/min. In detail, a torque command of 100 Nm has been applied with a slew rate of 5000 Nm/s. As shown in Fig. 21 (*a*), the controllers successfully follow the torque reference; however, the rotor current exhibits a pronounced undershoot at the transient onset. This behavior arises from the armature reaction between stator and rotor windings, which is particularly relevant for low rotor current levels. In detail, the underlying mechanism can be explained by expressing the rotor current as:

$$i_f = \frac{v_f - \frac{d}{dt}\lambda_f}{R_f} \simeq \frac{v_f - (\frac{di_f}{dt} \cdot l_{ff} + \frac{di_d}{dt} \cdot l_{fd})}{R_f} \tag{27}$$

Authorized licensed use limited to: Politecnico di Torino. Downloaded on May 26,2026 at 17:03:39 UTC from IEEE Xplore. Restrictions apply.
© 2026 IEEE. All rights reserved, including rights for text and data mining and training of artificial intelligence and similar technologies. Personal use is permitted, but republication/redistribution requires IEEE permission. See https://www.ieee.org/publications/rights/index.html for more information.

This article has been accepted for publication in IEEE Transactions on Power Electronics. This is the author's version which has not been fully edited and content may change prior to final publication. Citation information: DOI 10.1109/TPEL.2026.3696740

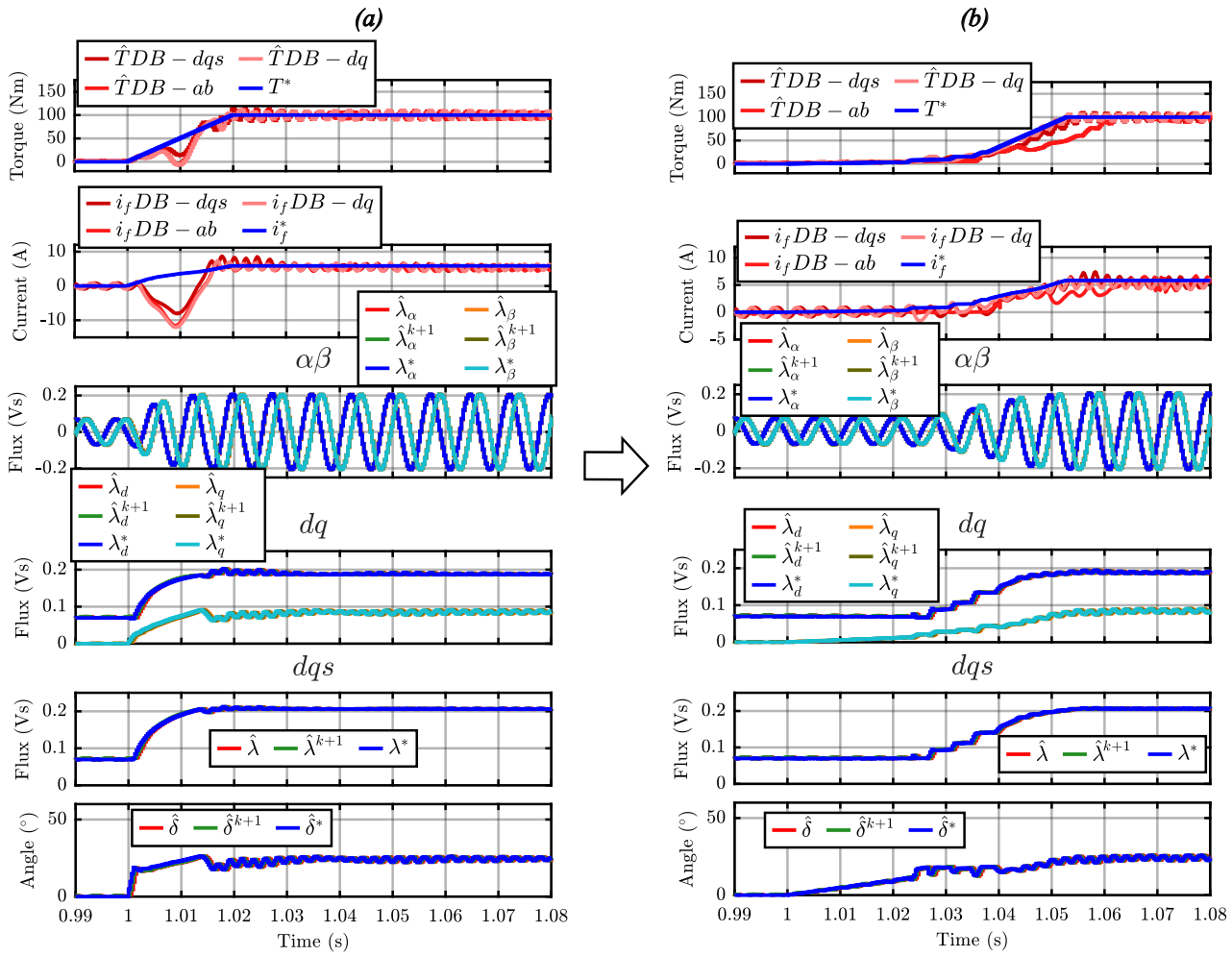


Fig. 21: Experimental results of torque transient response from 0 to 100 Nm, 5000 Nm/s, 4000 r/min: (a) without slew rate limitation for i_f <1 A; (b) with slew rate limitation at 150 Nm/s for i_f <1 A.

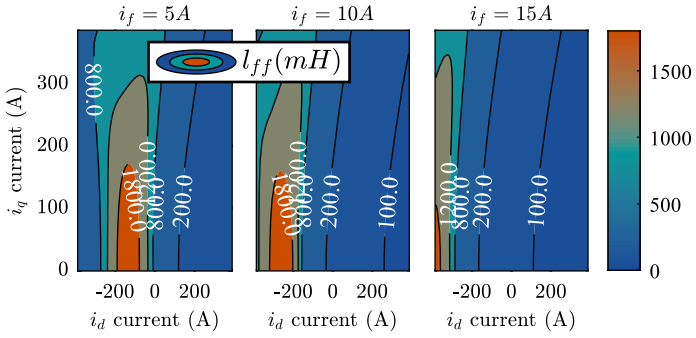


Fig. 22: Current-to-inductance l_{ff} map for the EESM under consideration.

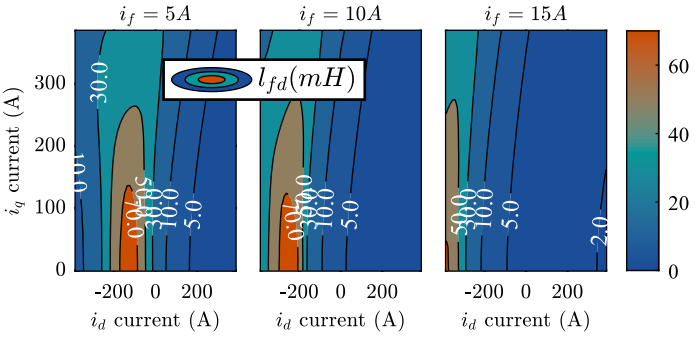


Fig. 23: Current-to-inductance l_{fd} map for the EESM under consideration.

where l_{ff} and l_{fd} are the rotor self-differential inductance and the cross-coupling differential inductance between the rotor and the stator d-axis, respectively. The cross-coupling differential inductance between the rotor and the stator q-axis, l_{fq}, is neglected in (27) because it is typically very small. Further details on this formulation are provided in [45].

As illustrated in Fig. 22 and Fig. 23, the rotor self-differential inductance l_{ff} is approximately two orders of magnitude larger than l_{fd}. However, requesting a very high torque slew rate starting from zero torque implies a rapid variation of the stator flux, which in turn results in a large positive slew rate of the stator d-axis current, as shown in Fig. 24. Under these conditions, the time derivative of the rotor flux $\frac{d}{dt}\lambda_f$ is predominantly affected by the stator d-axis current component through the term $l_{fd}\frac{di_d}{dt}$. From (27), it follows that a rapid positive variation of the stator d-axis current

Authorized licensed use limited to: Politecnico di Torino. Downloaded on May 26,2026 at 17:03:39 UTC from IEEE Xplore. Restrictions apply.
© 2026 IEEE. All rights reserved, including rights for text and data mining and training of artificial intelligence and similar technologies. Personal use is permitted, but republication/redistribution requires IEEE permission. See https://www.ieee.org/publications/rights/index.html for more information.

This article has been accepted for publication in IEEE Transactions on Power Electronics. This is the author's version which has not been fully edited and content may change prior to final publication. Citation information: DOI 10.1109/TPEL.2026.3696740

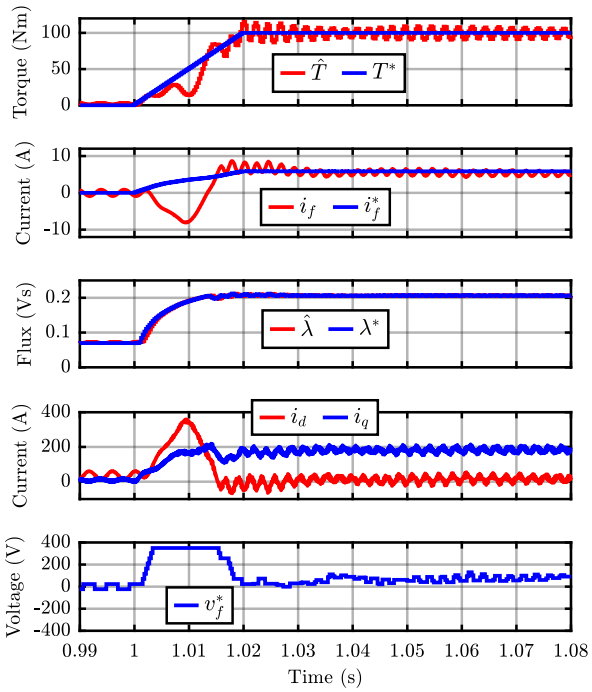


Fig. 24: Experimental results of torque transient response from 0 to 100 Nm, 5000 Nm/s, 4000 r/min using DB-dqs: view of the stator dq currents and the reference rotor voltage v_f^*.

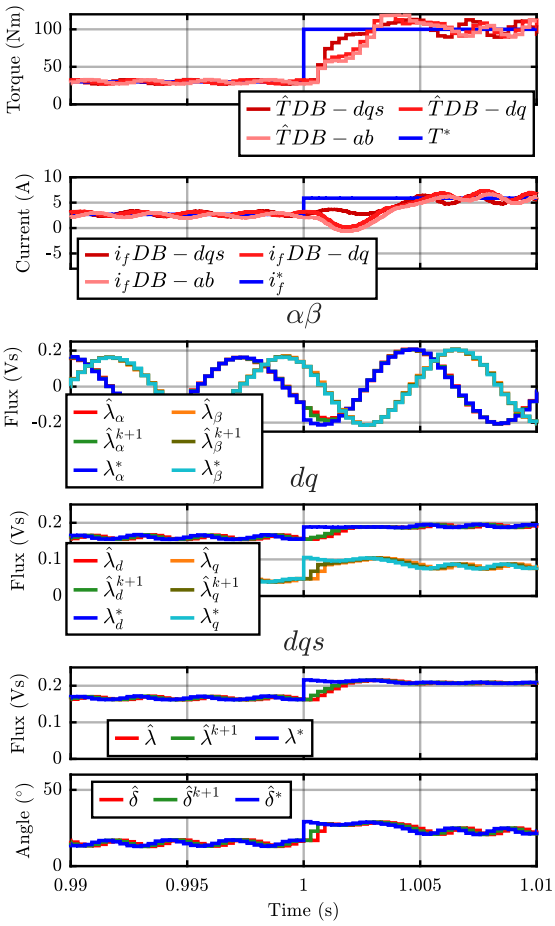


Fig. 25: Experimental results of torque step response from 30 to 100 Nm, 4000 r/min.

($\frac{di_d}{dt} \gg 0$) induces an opposing rotor back-emf that counteracts the controlled rotor voltage v_f. This may result in operating conditions where $\left|\frac{d}{dt}\lambda_f\right| > |v_f|$, thereby temporarily driving the rotor current i_f to negative values. In this condition, the rotor flux regulator uses all the available voltage to restore the rotor current i_f to its reference value, which leads to a temporary loss of controllability of the rotor current, as shown in Fig. 24.

To mitigate this effect, the slew-rate of the torque reference is limited to 150 Nm/s when the rotor current is lower than 1 A $i_f \leq 1$ A. The results shown in Fig. 21(b) confirm that this strategy stabilizes the rotor current regulation without significantly derating the dynamic performance of the torque controllers. Indeed, the slew rate of 150 Nm/s corresponds to achieving the machine's rated torque in less than 1 s.

It is highlighted that the decision to discretize the control LUTs by assuming only positive rotor current i_f values is a deliberate choice. This way, undershoots of rotor current i_f do not affect the outputs of the stator control LUTs, preventing dangerous interaction between the stator and rotor control loops that could lead to temporary uncontrollability of both.

The step-response test shown in Fig. 25 provides further validation of the dynamic performance of the proposed torque controllers. In this test, the torque reference is changed from 30 Nm to 100 Nm to avoid operation at the aforementioned limited torque slew rate. Although the available stator voltage margin does not allow a double-step torque response, the controllers achieve the target torque within the minimum number of sampling periods and without overshoots, according to the DB strategy. It is noted that the definition of different torque references for stator T^* and rotor T_f^* enables the stator control loops to deliver the fastest feasible torque response, while the rotor current/flux progressively converges to its steady-state value, thereby ensuring efficiency optimization.

In Fig. 25, it is noted that the estimated torque $\hat{T}$ exhibits small oscillations that are consistent with the transient behavior of the rotor current. Moreover, implementing the DB-DFC in the stator dqs reference frame yields a smaller rotor current undershoot at the onset of the torque transient than the other two DB approaches. This behaviour of DB-dqs is justified because the dqs coordinates exhibit decoupled voltage margins across the control axes. Indeed, stator flux amplitude regulation requires only a limited voltage margin (26), mitigating the interaction between the stator d-axis and the rotor current i_f.

The interaction between stator and rotor windings becomes even more critical when performing torque transients that drive the torque and rotor current toward zero. Indeed, torque zeroing requires reducing the stator flux to its minimum value, $\lambda_{\min} = 0.04$ Vs, which is arbitrarily defined to ensure proper operation of the stator flux observer. Consequently, the stator d-axis current approaches zero. However, due to the MUT's saliency, the d-axis current is negative under load conditions; therefore, when the torque is reduced toward zero, the derivative of the stator d-axis current $\frac{di_d}{dt}$ becomes positive. Recalling (27), it is evident that in this scenario the contribution of the controlled rotor voltage v_f and that of the cross-coupling term

Authorized licensed use limited to: Politecnico di Torino. Downloaded on May 26,2026 at 17:03:39 UTC from IEEE Xplore. Restrictions apply.
© 2026 IEEE. All rights reserved, including rights for text and data mining and training of artificial intelligence and similar technologies. Personal use is permitted, but republication/redistribution requires IEEE permission. See https://www.ieee.org/publications/rights/index.html for more information.

This article has been accepted for publication in IEEE Transactions on Power Electronics. This is the author's version which has not been fully edited and content may change prior to final publication. Citation information: DOI 10.1109/TPEL.2026.3696740

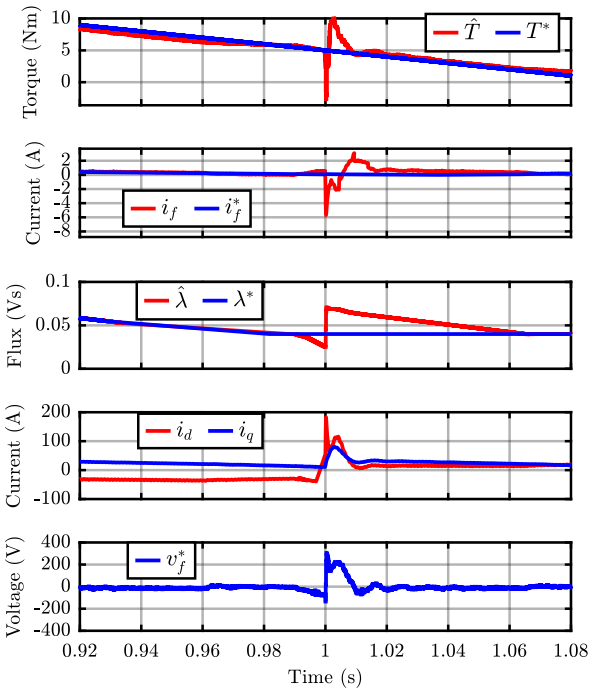


Fig. 26: Experimental results of torque transient from 50 to 0 Nm using DB-dqs, 50 Nm/s, 4000 r/min: magnification view of the stator dq currents and the reference rotor voltage v_f^*.

$l_{fd}\frac{di_d}{dt}$ share the same sign. However, if the rotor flux loop is not sufficiently fast to compensate for the additional negative voltage induced by the armature reaction, this condition may again result in an uncontrolled negative rotor current. The extent of this rotor current undershoot is directly related to the reaction time of the controller in detecting the undesired negative rotor current and consequently apply a positive rotor voltage. This behaviour is shown in Fig. 26, where the torque reference has been reduced from 50 Nm to 0 Nm with a slew rate of 50 Nm/s at a constant speed of 4000 r/min.

Moreover, the influence of the sampling frequency on the extent of the rotor current undershoot has been investigated, leading to the results presented in Fig. 27. It is noted that increasing the sampling frequency substantially attenuates the rotor current undershoot, which becomes negligible at a sampling frequency of $f_s = 10$ kHz. This improvement is attributed to the faster control response, which more effectively damps rotor current oscillations.

Although this effect is common to all considered DB approaches, distinct torque transient behaviors are observed at the same sampling frequency. These behaviors are shown in Fig. 28, where the torque reference is reduced from 150 Nm to 0 Nm with a slew rate of 1000 Nm/s at a constant speed of 4000 r/min, employing a sampling frequency of 10 kHz. The results presented in Fig. 28 still confirm that the DB-dqs approach features better dynamic performance for the MUT, as already highlighted in the analysis of the step response shown in Fig. 25.

3) Fast torque reversals: To further evaluate the dynamic of torque regulation featured by the proposed torque controllers, fast torque reversal tests have been conducted along the

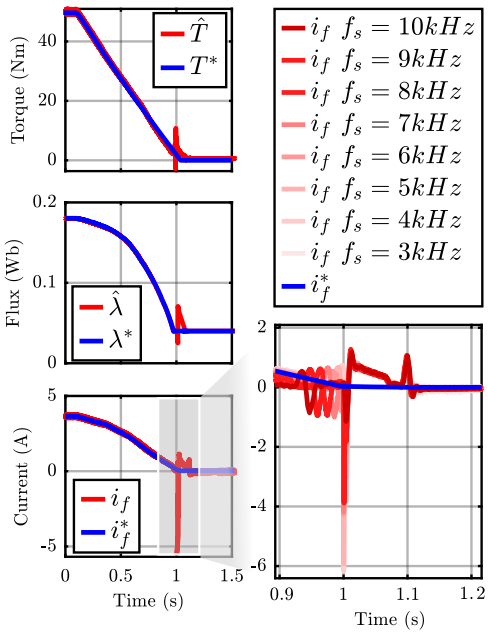


Fig. 27: Experimental results of torque transient from 50 to 0 Nm using DB-dqs, 50 Nm/s, 4000 r/min: effect of the sampling frequency.

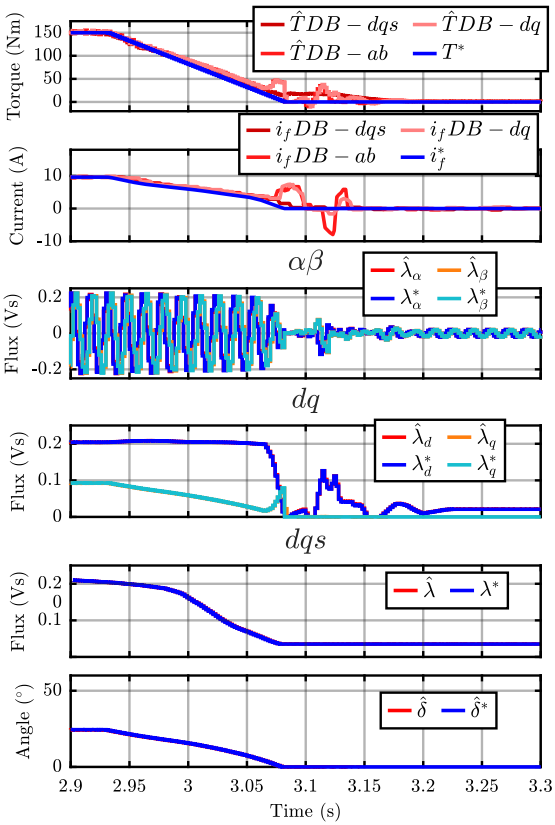


Fig. 28: Experimental results of torque transient from 150 to 0 Nm, 1000 Nm/s, 4000 r/min, $f_s = 10$ kHz (a downsampling of 1/20 is applied).

MTPS profile. Again, the MUT has been accelerated from standstill to 10000 r/min with an acceleration of approximately

Authorized licensed use limited to: Politecnico di Torino. Downloaded on May 26,2026 at 17:03:39 UTC from IEEE Xplore. Restrictions apply.
© 2026 IEEE. All rights reserved, including rights for text and data mining and training of artificial intelligence and similar technologies. Personal use is permitted, but republication/redistribution requires IEEE permission. See https://www.ieee.org/publications/rights/index.html for more information.

This article has been accepted for publication in IEEE Transactions on Power Electronics. This is the author's version which has not been fully edited and content may change prior to final publication. Citation information: DOI 10.1109/TPEL.2026.3696740

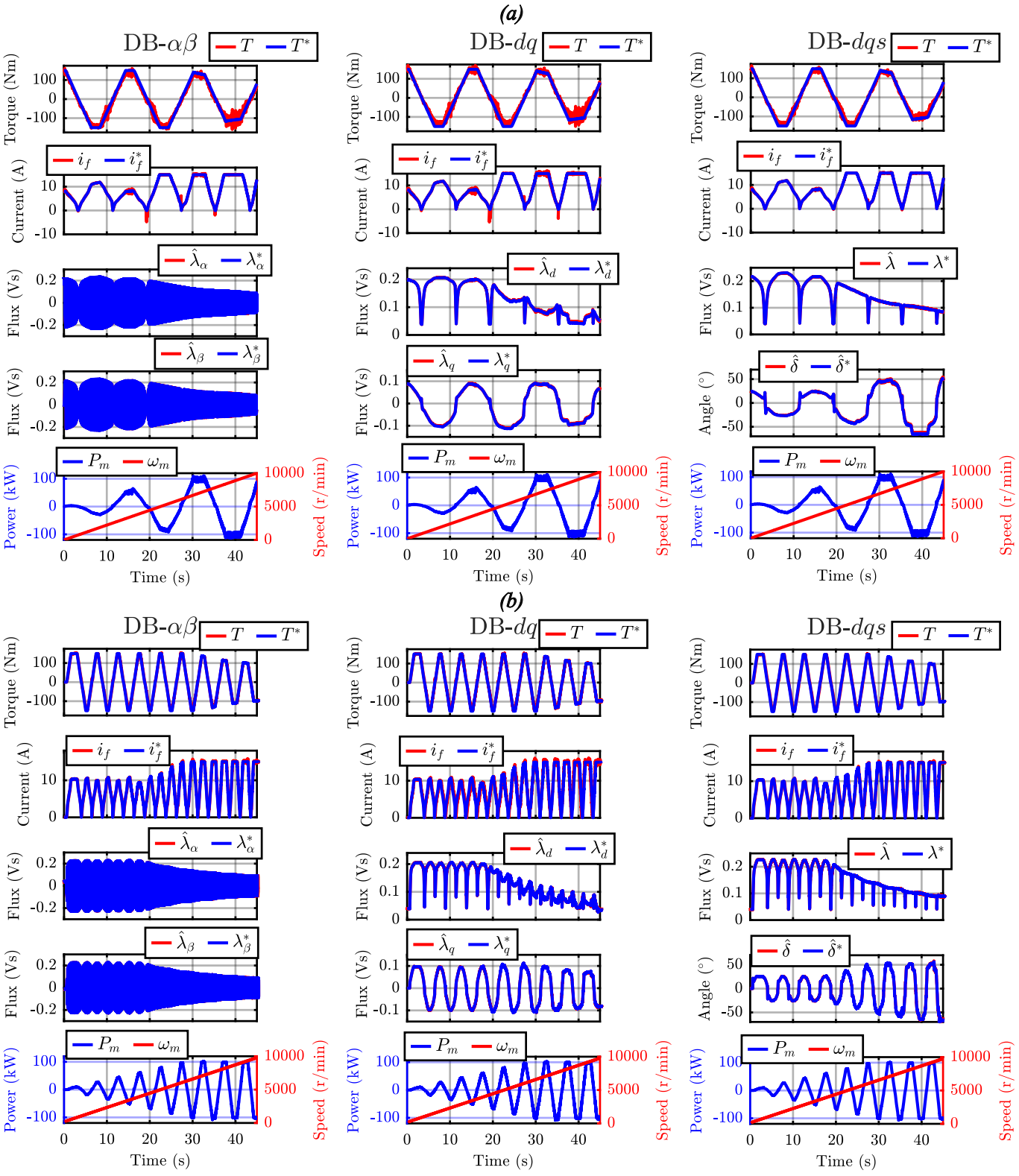


Fig. 29: Experimental results of fast torque reversals along the MTPS profile: (a) $f_s = 3$ kHz; (b) $f_s = 10$ kHz.

230 r/min/s, while the torque reference T^*_{in} has been set to 150 Nm. In this case, however, the torque reference has been periodically reversed to induce rapid transitions between motoring and braking modes.

For a sampling frequency of 3 kHz, the reversal frequency and torque slew rate have been set to 0.2 Hz and 50 Nm/s, respectively. As shown in Fig. 29 (a), the rotor current exhibits temporary, but not critical, uncontrollability when executing rapid torque reductions. This effect is justified by the previously made considerations on the results obtained when

Authorized licensed use limited to: Politecnico di Torino. Downloaded on May 26,2026 at 17:03:39 UTC from IEEE Xplore. Restrictions apply.
© 2026 IEEE. All rights reserved, including rights for text and data mining and training of artificial intelligence and similar technologies. Personal use is permitted, but republication/redistribution requires IEEE permission. See https://www.ieee.org/publications/rights/index.html for more information.

This article has been accepted for publication in IEEE Transactions on Power Electronics. This is the author's version which has not been fully edited and content may change prior to final publication. Citation information: DOI 10.1109/TPEL.2026.3696740

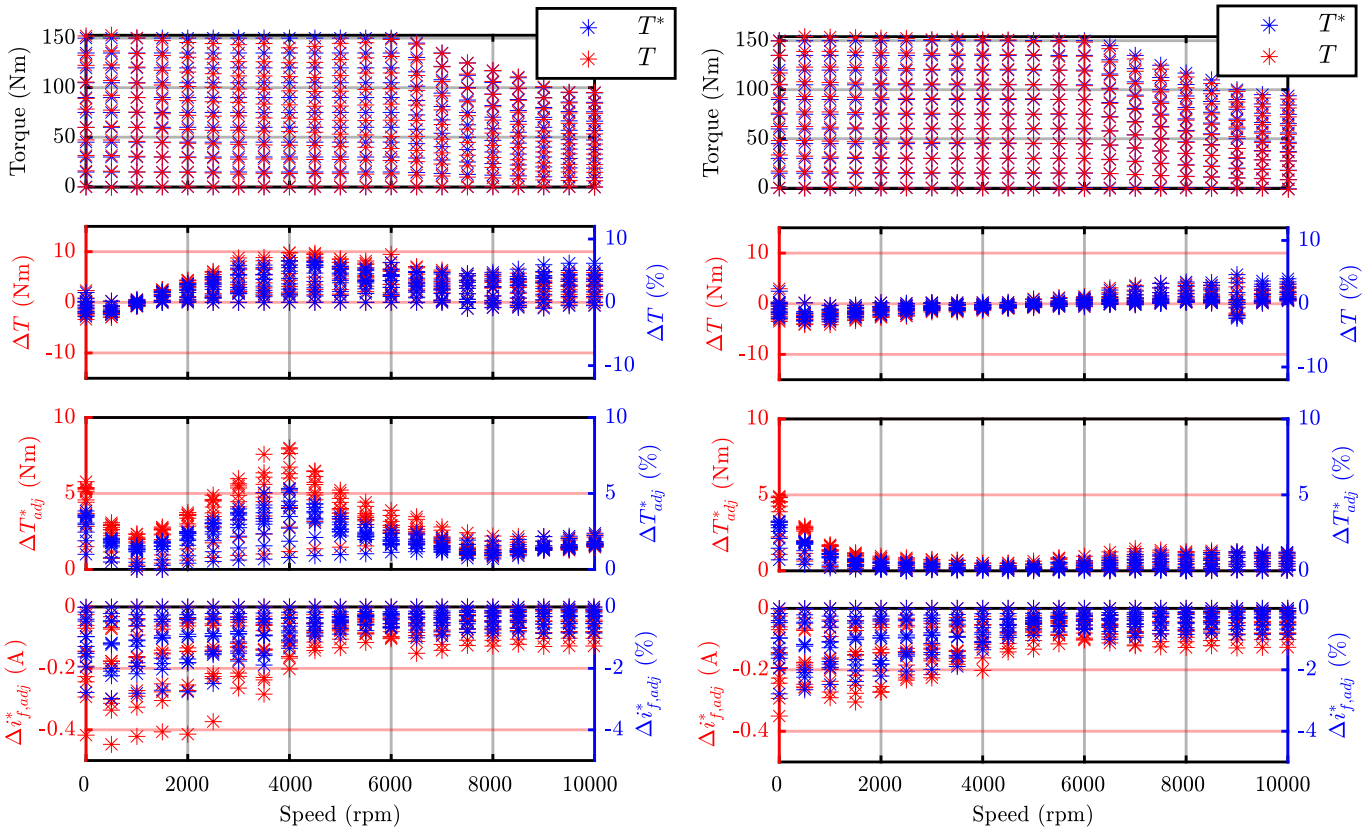


Fig. 30: Experimental results of steady-state torque accuracy using DB-dqs: (a) $f_s = 3$ kHz; (b) $f_s = 10$ kHz.

performing the torque transients that zeroing the torque (see Fig. 27 and Fig. 28). Nonetheless, increasing the sampling frequency to 10 kHz enabled higher reversal frequency (0.5 Hz) and torque slew rate (150 Nm/s), with only the mechanical constraints of the test rig limiting performance. Using this slope of torque reference, the maximum power of the machine under test (100 kW) has been reversed in about 1.2 s at the maximum speed of 10000 r/min, representing a very stressful test for automotive applications. Under these conditions, corresponding to typical operative sampling and switching frequency conditions, no uncontrollability phenomena of the rotor current have been reported (see Fig. 29 (b)).

In summary, the obtained results validate the robustness of the proposed DB-DFCs under severe dynamic stress conditions. The MUT maintained stable operation across the full speed range, including fast transitions between motoring and braking, with no overcurrent or instability events. Although operation at 3 kHz remains feasible, higher sampling frequencies yield superior dynamic torque performance, particularly when the rotor current must be rapidly nullified.

4) Steady-state torque accuracy: The steady-state torque regulation accuracy of the proposed controllers has been verified over the entire operating range of the MUT. The speed has been incremented in steps of 500 r/min, from standstill up to 10000 r/min, and at each speed level, ten equally spaced torque references have been applied between 0 and the limit torque T_{lim} clamped at 150 Nm. It is highlighted that no significant differences have been reported between the DB approaches in terms of steady-state torque accuracy, since the latter is related to the stator flux observer performance. However, the stator flux observer is the same for all considered DB approaches. Therefore, experimental results are reported only for the DB-dqs approach, which was arbitrarily selected among the three possibilities.

The obtained results, reported in Fig. 30, demonstrate torque accuracy regulation across all test conditions. The steady-state torque error ΔT, expressed in absolute terms and as a percentage of the torque limit T_{lim}, remained within acceptable bounds throughout the operating range. This confirms the high precision of the proposed DB-DFC in obtaining T^*, despite the absence of explicit compensation for iron and mechanical losses in the computation of λ^*,δ^* and i_f^*. At a sampling frequency of 3 kHz, a not negligible degradation in torque regulation accuracy has been reported (see Fig. 30 (a)), consistent with the well-known derating of torque controllability (discretization effects, huge current ripple, flux observer performance, etc.) given by the limited sampling-to-fundamental frequency ratio that reaches a value lower than 10 at the maximum speed. Nevertheless, it is noted how the torque regulation accuracy of the DB-DFC is extremely high when increasing the sampling frequency to a typical operative value of 10 kHz, as shown in Fig. 30 (b). Finally, the obtained high accuracy of torque regulation is surely justified by the implemented integral correction loops for the torque ΔT^*_{adj} and the rotor current $\Delta i^*_{f,adj}$ references, as shown in Fig. 30.

In the following, only the behaviour of the torque controllers

Authorized licensed use limited to: Politecnico di Torino. Downloaded on May 26,2026 at 17:03:39 UTC from IEEE Xplore. Restrictions apply.
© 2026 IEEE. All rights reserved, including rights for text and data mining and training of artificial intelligence and similar technologies. Personal use is permitted, but republication/redistribution requires IEEE permission. See https://www.ieee.org/publications/rights/index.html for more information.

This article has been accepted for publication in IEEE Transactions on Power Electronics. This is the author's version which has not been fully edited and content may change prior to final publication. Citation information: DOI 10.1109/TPEL.2026.3696740

at the sampling frequency of 10 kHz is described. Indeed, the reduction in torque controllability at a sampling frequency of 3 kHz makes it difficult to identify the causes of torque error, which, however, remains below 10% of the limit torque. Therefore, considering Fig. 30 (*b*), it is noted that at very low speed the adjustment of torque ΔT^*_{adj} reference is high since the impact of voltage errors is significant and not accounted for in (18), (19), (20), (21). In the medium-speed range, torque adjustment is reduced because the effects of voltage errors and iron losses are negligible. Consequently, the torque adjustment primarily accounts for detuning of the control maps. Finally, at high speeds, the torque adjustment increases because iron losses are partially compensated by the reliable feedback provided by the VI estimator of the stator flux observer. Regarding the adjustment of the rotor current reference, it is noted that it remains quite limited across the entire speed range. Indeed, the maximum rotor current adjustment is always less than 4% and mainly due to the detuning of the current-to-flux map from FEA providing the rotor flux reference from the corresponding rotor current one (see Fig. 7).

V. Conclusion

This article presented high-performance self-calibrated torque controllers for traction-oriented EESMs based on DB-DFC strategies implemented in different reference coordinates. The proposed solutions achieve high torque regulation accuracy across the entire torque–speed range while minimizing total Joule loss, accounting for both stator and rotor windings, without requiring any calibration procedures for the inner control loops. Besides, the proposed torque controllers achieve high dynamic torque regulation performances even at extremely low sampling-to-fundamental-frequency ratios. Therefore, the proposed torque controllers may offer a highly attractive solution for the traction industry, as they could enable straightforward certification procedures, drastically simplifying calibration.

Experimental validation was conducted on a commercial EESM for automotive applications, and the results confirmed the effectiveness of the proposed DB-DFC strategies in fully exploiting the machine's torque and constant-power speed-range capabilities, as well as their high accuracy in steady-state torque regulation. The experimental test campaign also reported the execution of fast torque transients at different sampling frequencies to highlight their impact on managing the significant armature reaction typically affecting EESMs. The results demonstrated that the lower the sampling frequency and the higher the torque rate transition, the greater the probability of temporary rotor current uncontrollability due to voltage constraints imposed by the exciter. However, the results obtained at typical sampling and switching frequencies showed that this effect is significantly mitigated, or even disappears, when realistic torque transients are performed. It is highlighted that establishing a priori quantitative stability boundaries is not straightforward, as they depend strictly on the EESM under consideration.

Future developments and improvements of this work include the following.

- The computation of stator and rotor flux references can be performed using frequency-dependent LUTs that minimize the machine's overall losses, accounting for the iron and mechanical losses contributions.
- The direct control of the stator flux vector can be performed by exploiting the deep overmodulation region of the inverter up to the six-step operation. This way, the machine could be operated at its potential maximum power for a given inverter's dc-link voltage.

Acknowledgment

The authors would like to acknowledge the support from the Power Electronics Innovation Center (PEIC) of Politecnico di Torino (www.peic.polito.it).

Appendix

The procedure to normalize and linearly interpolate LUT3, LUT4 and LUT5, thus generalizing the normalization procedures proposed in [30], [42] for PMSMs, is reported hereafter.

The implementation of LUT3, LUT4, and LUT5 is characterized by a strong coupling between the torque references and the secondary input variables. Specifically, the rotor torque reference T^*_f is constrained by the flux amplitude limit λ_{lim}, whereas the stator torque reference T^* is intrinsically linked to the instantaneous rotor current i_f according to the torque limit T_{lim}. Such interdependencies among the interpolation inputs lead to highly irregular map domains, posing significant challenges for real-time linear interpolation in digital controllers. To address these implementation constraints, the regularization technique proposed in [30], [42] for control maps of PMSMs has been considered and specifically extended for EESMs in this work. The core of this technique involves a normalization procedure where dependent input dimensions are mapped into a per-unit (pu) scale ranging from 0 to 1. Within this regularized domain the following rules are applied:

- A value of 0 pu represents the minimum physically admissible value of the variable for a given set of other inputs;
- A value of 1 pu represents the maximum physically admissible value of the variable for a given set of other inputs.

This transformation ensures that LUTs can be elaborated using standard linear interpolation methods while preserving the underlying nonlinear relationships. Consequently, the inputs for LUT3, LUT4, and LUT5 are derived through the per-unit normalization of the torque references to their instantaneous maximum capabilities:

$$T_{\text{pu}} = \frac{T^*}{T_{\text{lim}}}; \quad T_{f,\text{pu}} = \frac{T^*_f}{T_{\text{max}}}. \tag{28}$$

The regularized flux amplitude reference map (LUT3) is depicted in Fig. 31 for different rotor current i_f levels. Similarly, the load angle reference map (LUT4) is shown in Fig. 32. Finally, the rotor current reference map (LUT5) is illustrated in Fig. 33 as a function of the flux amplitude limit λ_{lim}.

Authorized licensed use limited to: Politecnico di Torino. Downloaded on May 26,2026 at 17:03:39 UTC from IEEE Xplore. Restrictions apply.
© 2026 IEEE. All rights reserved, including rights for text and data mining and training of artificial intelligence and similar technologies. Personal use is permitted, but republication/redistribution requires IEEE permission. See https://www.ieee.org/publications/rights/index.html for more information.

This article has been accepted for publication in IEEE Transactions on Power Electronics. This is the author's version which has not been fully edited and content may change prior to final publication. Citation information: DOI 10.1109/TPEL.2026.3696740

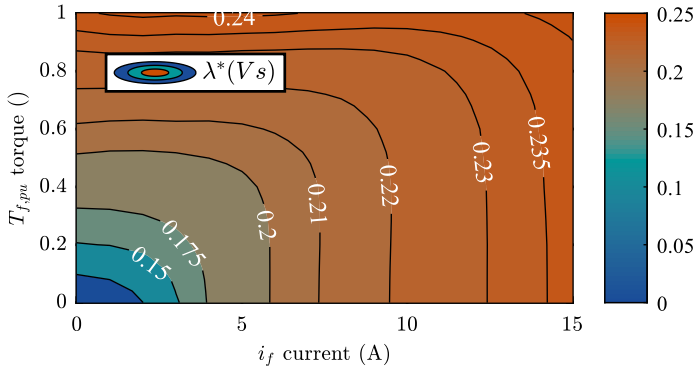


Fig. 31: Normalized flux amplitude reference (λ^*) map (LUT3) for the EESM under consideration.

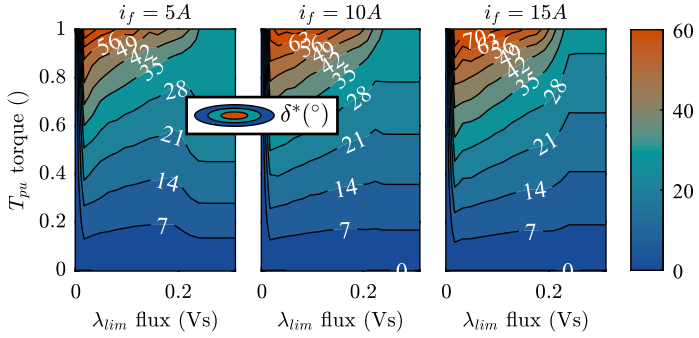


Fig. 32: Normalized load angle reference (δ^*) map (LUT4) for the EESM under consideration.

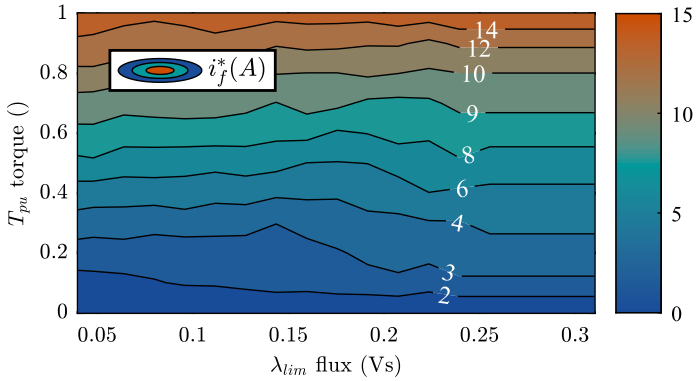


Fig. 33: Normalized rotor current reference (i_f^*) map (LUT5) for the EESM under consideration.

REFERENCES

[1] A. El-Refaie and M. Osama, "High specific power electrical machines: A system perspective," *CES Transactions on Electrical Machines and Systems*, vol. 3, no. 1, pp. 88–93, 2019.

[2] C. Rossi, D. Casadei, A. Pilati, and M. Marano, "Wound rotor salient pole synchronous machine drive for electric traction," in *Conference Record of the 2006 IEEE Industry Applications Conference Forty-First IAS Annual Meeting*, vol. 3, 2006, pp. 1235–1241.

[3] F. Graffeo, S. Vaschetto, M. Cossale, M. Kerschbaumer, E. C. Bortoni, and A. Cavagnino, "Cylindrical wound-rotor synchronous machines for traction applications," in *2020 International Conference on Electrical Machines (ICEM)*, vol. 1, 2020, pp. 1736–1742.

[4] F. Graffeo, S. Vaschetto, A. Tenconi, and A. Cavagnino, "No-load characteristic computation for wound field synchronous propulsion motors," in *2023 IEEE International Conference on Electrical Systems for Aircraft, Railway, Ship Propulsion and Road Vehicles and International Transportation Electrification Conference (ESARS-ITEC)*, 2023, pp. 1–6.

[5] ——, "Fast sizing procedure for salient-pole wound field synchronous motors for transportation electrification," in *2023 IEEE International Electric Machines and Drives Conference (IEMDC)*, 2023, pp. 1–7.

[6] M. Märgner and W. Hackmann, "Control challenges of an externally excited synchronous machine in an automotive traction drive application," in *2010 Emobility - Electrical Power Train*, 2010, pp. 1–6.

[7] R. Breda, E. Colavitto, S. Calligaro, R. Petrella, and B. Sarlioglu, "Model predictive control for wound rotor synchronous machines based on closed-form solution and fixed switching frequency," in *2024 IEEE Energy Conversion Congress and Exposition (ECCE)*, 2024, pp. 6349–6356.

[8] R. Breda, G. Andrioli, S. Calligaro, and R. Petrella, "Extended mtpa and flux-weakening control with total copper loss minimisation and transient torque compensation for wound-rotor synchronous machines," in *2023 IEEE Energy Conversion Congress and Exposition (ECCE)*, 2023, pp. 4829–4836.

[9] R. Breda, N. Andreon, S. Calligaro, and R. Petrella, "Comprehensive flux-weakening and analytical extended mtpa control featuring transient torque compensation for hybrid excited synchronous machines," in *2024 IEEE Energy Conversion Congress and Exposition (ECCE)*, 2024, pp. 6417–6424.

[10] L. Geier, S. Goehner, J. Stoss, A. Liske, and M. Hiller, "A novel highly dynamic torque control scheme for electrically excited synchronous machines," in *2024 IEEE 9th Southern Power Electronics Conference (SPEC)*, 2024, pp. 1–7.

[11] K. D. Hoang and H. K. A. Aorith, "Online control of ipmsm drives for traction applications considering machine parameter and inverter nonlinearities," *IEEE Transactions on Transportation Electrification*, vol. 1, no. 4, pp. 312–325, 2015.

[12] H. A. A. Awan, Z. Song, S. E. Saarakkala, and M. Hinkkanen, "Optimal torque control of saturated synchronous motors: Plug-and-play method," *IEEE Transactions on Industry Applications*, vol. 54, no. 6, pp. 6110–6120, 2018.

[13] E. Trancho, E. Ibarra, A. Arias, C. Salazar, I. Lopez, A. D. de Guereñu, and A. Peña, "Ipmsm torque control strategies based on luts and vct feedback for robust control under machine parameter variations," in *IECON 2016 - 42nd Annual Conference of the IEEE Industrial Electronics Society*, 2016, pp. 2833–2838.

[14] V. Manzolini, D. Da Rù, and S. Bolognani, "An effective flux weakening control of a syrm drive including mtpv operation," *IEEE Transactions on Industry Applications*, vol. 55, no. 3, pp. 2700–2709, 2019.

[15] I. Boldea, M. C. Paicu, and G.-D. Andreescu, "Active flux concept for motion-sensorless unified ac drives," *IEEE Transactions on Power Electronics*, vol. 23, no. 5, pp. 2612–2618, 2008.

[16] A. K. Jain and V. T. Ranganathan, "Modeling and field oriented control of salient pole wound field synchronous machine in stator flux coordinates," *IEEE Transactions on Industrial Electronics*, vol. 58, no. 3, pp. 960–970, 2011.

[17] A. Ionta, S. Rubino, F. Graffeo, and R. Bojoi, "Unified torque control of electrically excited synchronous machines for traction applications," in *2025 IEEE Industry Applications Society Annual Meeting (IAS)*, 2025, pp. 1–8.

[18] A. Ionta, S. Rubino, F. Mandrile, F. Graffeo, R. Bojoi, and E. Armando, "Direct flux vector control of electrically excited synchronous machines for electrical vehicles," in *2024 IEEE Energy Conversion Congress and Exposition (ECCE)*, 2024, pp. 6431–6438.

[19] B. Kenny and R. Lorenz, "Stator- and rotor-flux-based deadbeat direct torque control of induction machines," *IEEE Transactions on Industry Applications*, vol. 39, no. 4, pp. 1093–1101, 2003.

[20] J. S. Lee, C.-H. Choi, J.-K. Seok, and R. D. Lorenz, "Deadbeat-direct torque and flux control of interior permanent magnet synchronous machines with discrete time stator current and stator flux linkage observer," *IEEE Transactions on Industry Applications*, vol. 47, no. 4, pp. 1749–1758, 2011.

[21] Y. Nie, I. P. Brown, and D. C. Ludois, "Deadbeat-direct torque and flux control for wound field synchronous machines," *IEEE Transactions on Industrial Electronics*, vol. 65, no. 3, pp. 2069–2079, 2018.

[22] Y. Nie, D. C. Ludois, and I. P. Brown, "Deadbeat-direct torque and flux control of wound field synchronous machine at low sampling to fundamental frequency ratios," *IEEE Transactions on Industry Applications*, vol. 55, no. 4, pp. 3813–3822, 2019.

[23] Y. Kim and K. Nam, "Copper-loss-minimizing field current control

Authorized licensed use limited to: Politecnico di Torino. Downloaded on May 26,2026 at 17:03:39 UTC from IEEE Xplore. Restrictions apply.
© 2026 IEEE. All rights reserved, including rights for text and data mining and training of artificial intelligence and similar technologies. Personal use is permitted, but republication/redistribution requires IEEE permission. See https://www.ieee.org/publications/rights/index.html for more information.

This article has been accepted for publication in IEEE Transactions on Power Electronics. This is the author's version which has not been fully edited and content may change prior to final publication. Citation information: DOI 10.1109/TPEL.2026.3696740

scheme for wound synchronous machines," *IEEE Transactions on Power Electronics*, vol. 32, no. 2, pp. 1335–1345, 2017.

[24] M.-R. Park, D.-M. Kim, Y.-H. Jung, M.-S. Lim, and J.-P. Hong, "Modeling, design and control of wound-field synchronous motor for high energy efficiency of electric vehicle," in *2019 IEEE Energy Conversion Congress and Exposition (ECCE)*, 2019, pp. 3960–3967.

[25] C. D. Nguyen and W. Hofmann, "Self-tuning adaptive copper-losses minimization control of externally excited synchronous motors," in *2014 International Conference on Electrical Machines (ICEM)*, 2014, pp. 897–902.

[26] C. Zaghrini, G. Khoury, M. Fadel, R. Ghosn, and F. Khatounian, "Minimum copper losses per torque optimization on electrically excited synchronous motors for electric vehicles applications," in *2022 IEEE 20th International Power Electronics and Motion Control Conference (PEMC)*, 2022, pp. 661–666.

[27] S. Müller and N. Parspour, "Applying a measurement-based iron loss model to an efficiency optimized torque control of an electrically excited synchronous machine," in *2020 International Conference on Electrical Machines (ICEM)*, vol. 1, 2020, pp. 779–785.

[28] H. El Khatib, D. Gerling, and M. Saur, "Deadbeat flux vector control as a one single control law operating in the linear, overmodulation, and six-step regions with time-optimal torque control," *IEEE Open Journal of Industry Applications*, vol. 3, pp. 247–270, 2022.

[29] H. A. A. Awan, S. E. Saarakkala, and M. Hinkkanen, "Flux-linkage-based current control of saturated synchronous motors," *IEEE Transactions on Industry Applications*, vol. 55, no. 5, pp. 4762–4769, 2019.

[30] S. Rubino, L. Tolosano, F. Mandrile, E. Armando, and R. Bojoi, "Flux polar control (fpc): A unified torque controller for ac motor drives," *IEEE Transactions on Industry Applications*, vol. 59, no. 4, pp. 4140–4163, 2023.

[31] S.-K. Sul, *Control of Electric Machine Drive Systems*. New York, NY, USA: Wiley-IEEE Press, 2011.

[32] G. Pellegrino, R. Bojoi, and P. Guglielmi, "Unified direct-flux vector control for ac motor drives," *IEEE Transactions on Industry Applications*, vol. 47, no. 5, pp. 2093–2102, 2011.

[33] A. Hava, R. Kerkman, and T. Lipo, "Simple analytical and graphical methods for carrier-based pwm-vsi drives," *IEEE Transactions on Power Electronics*, vol. 14, no. 1, pp. 49–61, 1999.

[34] A. Vagati, M. Pastorelli, G. Franceschini, and V. Drogoreanu, "Flux-observer-based high-performance control of synchronous reluctance motors by including cross saturation," *IEEE Transactions on Industry Applications*, vol. 35, no. 3, pp. 597–605, 1999.

[35] G. Pellegrino, R. I. Bojoi, P. Guglielmi, and F. Cupertino, "Accurate inverter error compensation and related self-commissioning scheme in sensorless induction motor drives," *IEEE Transactions on Industry Applications*, vol. 46, no. 5, pp. 1970–1978, 2010.

[36] E. Armando, R. Bojoi, P. Guglielmi, G. Pellegrino, and M. Pastorelli, "Experimental identification of the magnetic model of synchronous machines," *IEEE Transactions on Industry Applications*, vol. 49, no. 5, pp. 2116–2125, 2013.

[37] S. Goehner, J. Stoss, M. Brodatzki, B. Bachowsky, A. Liske, J. Kolb, and M. Hiller, "Combining locked rotor and steady state tests for eesm flux linkage identification," in *2024 IEEE 9th Southern Power Electronics Conference (SPEC)*, 2024, pp. 1–6.

[38] C. W. Secrest, D. S. Ochs, and B. S. Gagas, "Deriving state block diagrams that correctly model hand-code implementation—correcting the enhanced luenberger style motion observer as an example," *IEEE Transactions on Industry Applications*, vol. 56, no. 1, pp. 826–836, 2020.

[39] I. Bojoi, E. Armando, G. Pellegrino, and S. Rosu, "Self-commissioning of inverter nonlinear effects in ac drives," in *2012 IEEE International Energy Conference and Exhibition (ENERGYCON)*, 2012, pp. 213–218.

[40] H. El Khatib, D. Gaona, D. Gerling, and M. Saur, "Src as a reliable methodology to evaluate flux observer estimation accuracy," in *2020 IEEE 21st Workshop on Control and Modeling for Power Electronics (COMPEL)*, 2020, pp. 1–8.

[41] S.-Y. Kim, C. Choi, K. Lee, and W. Lee, "An improved rotor position estimation with vector-tracking observer in pmsm drives with low-resolution hall-effect sensors," *IEEE Transactions on Industrial Electronics*, vol. 58, no. 9, pp. 4078–4086, 2011.

[42] B.-H. Bae, N. Patel, S. Schulz, and S.-K. Sul, "New field weakening technique for high saliency interior permanent magnet motor," in *38th IAS Annual Meeting on Conference Record of the Industry Applications Conference, 2003.*, vol. 2, 2003, pp. 898–905 vol.2.

[43] F. Graffeo, S. Ferrari, S. Rubino, S. Vaschetto, and G. Pellegrino, "A scaling procedure for electrically-excited synchronous machines utilizing flux and loss maps," in *2024 International Conference on Electrical Machines (ICEM)*, 2024, pp. 1–8.

[44] F. Graffeo, S. Vaschetto, S. Rubino, A. Tenconi, and A. Cavagnino, "Fast computation of the no-load characteristic for wound field synchronous propulsion motors," *IEEE Transactions on Transportation Electrification*, vol. 11, no. 1, pp. 4111–4120, 2025.

[45] A. Ionta, S. Rubino, F. Graffeo, and R. Bojoi, "High-fidelity voltage-behind-reactance model of electrically excited synchronous machines using flux maps," *IEEE Open Journal of Industry Applications*, vol. 6, pp. 603–618, 2025.

Authorized licensed use limited to: Politecnico di Torino. Downloaded on May 26,2026 at 17:03:39 UTC from IEEE Xplore. Restrictions apply.
© 2026 IEEE. All rights reserved, including rights for text and data mining and training of artificial intelligence and similar technologies. Personal use is permitted, but republication/redistribution requires IEEE permission. See https://www.ieee.org/publications/rights/index.html for more information.